# Joint Centre for Mesoscale Meteorology, Reading, UK

## Collected preprints of papers submitted to the COST-75 International Seminar on Advanced Weather Radar Systems, Brussels, 20-23 September 1994

**Internal Report No. 36**

**November 1994**

**Met Office** Joint Centre for Mesoscale Meteorology Department of Meteorology
University of Reading PO Box 243 Reading RG6 6BB United Kingdom
Tel: +44 (0)118 931 8425 Fax: +44 (0)118 931 8791
www.metoffice.com

# CONTENTS

# REPORT OF COST 75 WORKING GROUP THREE: MULTIPARAMETER RADARS

A J Illingworth, Chairman of Cost 75, Working Group Three
JCMM, U of Reading, UK, RG6 2AU, FAX 44 734 35 26 04.
email: ajilling@met.rdg.ac.uk

## 1. INTRODUCTION

Most operational weather radars transmit at a single frequency and measure the intensity and the Doppler shift of the return power. Working group three is concerned with the additional information available from multiparameter radars which exploit either the polarisation properties of the radar returns or compare the return power at several different frequencies. We are fortunate in Europe to have several powerful multiparameter radars which are currently used for research; the time is now ripe to consider whether such techniques are appropriate for incorporation within future operational radar networks.

Working group three has identified two particular themes where multiparameter radars could have the most benefit in an operational environment:

i) Improved estimates of rainfall rates at the ground, and

ii) Identification of severe weather hazards, such as hail.

Many published research papers indicate how multiparameter techniques can contribute to these two topics, but it has still to be demonstrated that they can produce a positive and economic impact in an operational environment. Recently there have been several extensive field programs accompanied by independent validation, including two financed by the CEC, which provide the data sets to assess the potential benefits. A workshop is being organised for July 1995 to analyse the results of these campaigns with the specific aim of quantifying the improvements the multiparameter techniques can make in the operational environment.

In sections two and three of this report we summarise the new parameters available from polarisation diversity and multiple frequency radars, respectively, and discuss how they can contribute to the two themes identified above. In section four we give brief specifications of some of the existing multiparameter research radars in Europe and the programs they are involved in. Section five lists some of the outstanding problems to be tackled during the remainder of the COST action. The working group has produced 30 of the working documents (WD) for this COST action, so, in the interests of brevity, we have referred to these WDs rather than weigh this introductory review down with a long list of references.

The working group has focused on two themes, but this does not exhaust the potential applicability of multiparameter radars. The new techniques can be used to identify and characterise the various types of hydrometeors present within precipitation areas, and, as an example, these data can be used to advance our understanding of precipitation mechanisms and to validate and improve their representation within mesoscale models. There is also the possibility of identifying those regions containing supercooled liquid cloud droplets which pose a risk of aircraft icing. The multiparameter techniques may well be useful for spaceborne instruments on satellites. However, these aspects are judged to be outside the remit of the COST action.

*Cost-75 International Seminar on Advanced Weather Radar Systems*
*Brussels, 20-23 September 1994*
*To be published in 1995*

## 2.1 POLARISATION TECHNIQUES

The number of additional parameters available from polarisation diversity radars can appear bewildering. We shall initially consider linear polarisation, as this is used by most radars in Europe. A parallel set of variables exists for circular polarisation and observations made using one polarisation basis can, in theory, be converted to the other.

A radar transmitting pulses which are alternately horizontally and vertically polarised can measure $Z_H$ and $Z_V$, the reflectivities for the two polarisations, and with the addition of a cross-polar receiver the orthogonal reflectivity $Z_{VH}$ can be recorded. If the radar is Dopplerised then the difference in the phases of the returns in the two polarisations ($\phi_{DP} = \phi_V - \phi_H$) can be estimated.

We can now define the three major parameters for a linearly polarised radar:

a) The differential reflectivity, $Z_{DR} = 10 \log (Z_H/Z_V)$, senses the mean shape of the hydrometeors. Raindrops are oblate to a degree which depends upon their size, so $Z_{DR}$ is a measure of mean raindrop size and a combination of Z and $Z_{DR}$ provides an estimate of the drop size distribution which should yield a more accurate rainfall rate than from Z alone. Interpretation of $Z_{DR}$ for ice is more difficult.

b) The linear depolarisation ratio, $LDR = 10 \log(Z_{VH}/Z_H)$, is a measure of the fall mode of the precipitation. The highest cross-polar returns are associated with particles which are both wet and oblate and tumble as they fall. LDR is an excellent detector of wet ice. In convective clouds LDR can locate regions of small hail particles which are wet, and in stratiform rain LDR can identify melting snow which causes the enhanced reflectivity known as the 'bright band'.

c) The specific differential phase shift, $K_{DP}$, the rate of change of $\phi_{DP}$ with range, is a propagation effect. As the radar wave advances through a region containing oblate raindrops, a larger phase delay is introduced to the horizontally polarised wave. In theory $K_{DP}$ is more closely related to the rainfall rate than Z. In severe thunderstorms, the value of Z is dominated by the returns from the hail. $K_{DP}$ may provide a better estimate of rain rate as it responds only to the raindrops; hailstones tumble as they fall and so do not contribute to $K_{DP}$.

It is also possible to define various correlation parameters between the time series of the fluctuating radar reflectivity estimates, but, although this is an area of active research, it seems premature to recommend their implementation in an operational environment.

We now outline how observations of these parameters could contribute to the two themes identified in section one.

A) MORE ACCURATE MEASUREMENTS OF RAINFALL (WD 7, 14, 30).

i) If the radar beam is dwelling in the rain then a combination of Z and $Z_{DR}$ can, in theory, provide a better rain rate estimate than Z alone. In the heavier rain $K_{DP}$ may offer an improvement over Z.

ii) The vertical profile of radar reflectivity causes the major errors in rainfall estimates made with conventional radars; in this case the radar beam is often not in the rain and the inferred rainfall rate may be too high if the beam is in the bright band, or too low if it is in the ice above the bright band. Polarisation techniques (such as LDR) may provide information on the vertical profile by clearly identifying the bright band.

iii) Conventional radars can have difficulties identifying ground clutter and, in particular, anomalous propagation but polarisation parameters appear to locate them unambiguously.

iv) In severe storms, the presence of hail makes the magnitude of Z an unreliable measure of rainfall. $K_{DP}$ may provide a better rain rate estimate as it responds only to the contribution of the raindrops.

B) IDENTIFICATION OF SEVERE WEATHER HAZARDS SUCH AS HAIL (WD 33,53)

The ability of $K_{DP}$ to identify hail in a mixture of rain and hail has been described above. In addition there are some polarisation parameters which are sensitive to the onset of Mie scattering, which occurs for a particle size of about 1cm at C-band, and so could be used to locate regions of damaging hail within a storm.

## 2.2 ASPECTS OF POLARISATION REQUIRING FURTHER INVESTIGATION

The previous section suggests some important contributions that the new polarisation parameters can make in an operational environment. At this stage it is appropriate to identify various unresolved problems:

i) Propagation and attenuation at C-band (WD 29, 52).

At S-band (10cm) the interpretation of the polarisation parameters is relatively straightforward, but operational radars in Europe operate at C-band (5cm) and the increased attenuation leads to complications: the greater attenuation of the horizontally polarised beam can cause $Z_{DR}$ to become increasingly negative with range; depolarisation of the incident beam means that values of LDR rise with range, but $K_{DP}$ should be relatively immune to these effects. Once the magnitude of the problem has been quantified there are two possible approaches. It may be possible to correct for these propagation effects, or, alternatively, to exploit them and derive some additional path integrated information.

ii) Dwell time, accuracy of estimates and calibration (WD 50).

It is crucial to specify the precision required of the polarisation parameters in proposed operational algorithms. Radar estimates always have an inherent noise associated with then, and increased accuracy is generally achieved by longer dwell times or spatial integration. The additional information from the polarisation measurements must be carefully balanced against any losses in temporal and spatial resolution. The stability of hardware calibrations must be specified.

iii) Circular, linear or slant linear polarisation (WD 27, 51).

A parallel series of parameters exists for circular polarisation, and, in theory, it is possible to convert data sets from one polarisation basis to another. However, the effect of the inherent noise of the estimators can be different, as can propagation effects. At present it is not clear if linear or circular is the optimum solution, although most polarisation diversity radars in Europe use linear polarisation. Additional information may be available if the orthogonal polarisations are at directions other than the vertical and horizontal. A sequence of several 'slant linear' observations at different angles implies an increased dwell time.

v) Antenna limitations (WD 30).

Many polarisation measurements rely on detecting the small difference between two signals. Errors due to mismatched antenna sidelobes can arise when there are high gradients of reflectivity. The cross-polar antenna isolation limits the values of LDR which can be detected. We need to consider if techniques developed on research radars can be transferred to operational radars with antennas of lower specification.

## 3. DUAL FREQUENCY TECHNIQUES

If two or more frequencies are used then it is possible to gain additional information about the precipitation target (WD 31, 49). We can identify three specific benefits.

i) Reduction of dwell time.

If different frequencies are used for the transmitted pulse, then more independent samples can be obtained within a given dwell time and the errors in the radar estimates can generally be reduced. The use of FM/CW techniques enables a much lower peak power to be transmitted (WD 55). Both of these topics are being dealt with by working group four.

ii) Differential attenuation.

A comparison of the radar reflectivities at two wavelengths can be used to estimate the differential attenuation. This attenuation can then be related to the volume of liquid water present, whereas ice tends to have a much lower attenuation. One application is remote detection of icing hazard.

iii) Hail detection through Mie scattering.

If Mie scattering occurs only at the shorter wavelength then a comparison of the reflectivity values at the two wavelengths can be used to estimate the size of the precipitating particles. This method has been proposed for hail detection.

The most promising application of multi-frequency techniques for the goals of COST75 is the detection of hail and associated severe weather (WD 49). We can, however, identify three difficulties:

a) In storms which may contain hail, liquid precipitation is likely to result in severe attenuation at the shorter wavelength which will cause the dual wavelength ratio to fall below unity.

b) The reflectivity values of wet and dry hail can be very different; once well into the Mie region the cross-sections oscillate with increasing size.

c) It is important that the two beamwidths be well matched otherwise reflectivity gradients will dominate any variations in the dual wavelength ratio.

## 4. MULTIPARAMETER RADARS IN EUROPE.

The following table summarises the characteristics of some of the multiparameter radars in Europe. It is not intended to be exhaustive but has been extracted from the various working documents. Unless otherwise stated the radars operate at 5cm (C-band), have a beamwidth of about 1°, use linear polarisation and can measure $Z_{DR}$. The ability to measure $K_{DP}$ implies a Doppler capability.

| *WD* | *INSTITUTE, NAME OF RADAR* | *PARAMETERS AND COMMENTS* |
|---|---|---|
| 1,3 | Austria, Graz, 'IAS/ESA' | LDR. |
| 13 | Germany, DLR 'Poldirad' | LDR, $K_{DP}$, circular and slant polarisation. |
| 35 | Netherlands, Delft, 'DARR' | 10cm, Doppler, FM-CW, and LDR |
| 36 | Hungary, Budapest, 'MLR5' | 10cm (1.5°) and 3cm (0.5°), no polarisation. |
| 6 | UK, Chilbolton | 10cm, 0.25°, LDR and $K_{DP}$. |
| 6 | France, OPGC, 'Anatol' | 10cm, 2° beam, |
| 20,22 | Italy | Seven Doppler radars some with $K_{DP}$. |

Two CEC projects are supporting the field programs which involve the DLR radar and the several of the Italian radars:

i) PADRE 'Polarisation and Doppler Radar Experiment' (EV5V - CT92 - 0181) is analysing these techniques for qualitative and quantitative precipitation monitoring in severe weather (WD 17).

ii) Flood hazard control by multi-sensor storm tracking in Mediterranean areas. (EV5V-CT92-0167, described in WD43)

In addition there has been an extensive field program 'Cleopatra' (WD 32) with the DLR 'Poldirad' radar and considerable data has also been gathered in Eastern Europe using the dual wavelength MLR-2 radars from the former Soviet Union to detect hail.

## 5. OUTSTANDING PROBLEMS

The workshop planned for July 1995 will analyse the data from field studies using multiparameter radars with the aim of quantifying the benefits that the new techniques can bring to the two themes:
i) the quantitative estimation of surface rainfall and
ii) the detection of severe weather such as hail.

A key element is the validation by ground truth using rain gauges (WD 54) and direct observations of hail. In the past, case studies have been analysed which show a positive impact; the goal of the workshop is to show that these benefits can be demonstrated over a longer statistical period of observations and to define the algorithms used to achieve this. In addition, we must consider any improved performance of conventional radars, particularly when supplemented by the next generation of high resolution geostationary satellite data, and balance it against the advantages of the multiparameter radars.

In parallel with these validation studies, the workshop will aim to provide a quantitative appraisal of:
i) Correction and/or exploitation of propagation and attenuation at C-band.
ii) Required dwell time, accuracy and calibration procedures for the new parameters.
iii) Choice of polarisation bases, circular, linear or slant linear.
iv) Antenna specifications.

Finally, we must consider the effects of increased hardware complexity on system reliability when operating at remote unmanned sites. In addition, the multiparameter algorithms developed on a research radar may be quite complex, and we need to examine how they could be implemented in a semi-automatic operational environment and the degree of training that would be required.

**Acknowledgements.** All members of working group three have contributed to the work reported here: Dombai, Chandra, Holt, Meischner, Randeu, Scarchilli, Van Gorp, Vezzani.

# IMPROVED MEASUREMENTS OF RAINFALL USING DIFFERENTIAL PHASE TECHNIQUES

M. Blackman, JCMM, Univ of Reading, UK, fax: 44 734 352604
e-mail: markb@met.rdg.ac.uk
A.J. Illingworth, JCMM, Univ of Reading, UK, fax: 44 734 352604
e-mail: ajilling@met.rdg.ac.uk

## Introduction

Differential phase techniques offer the potential for improved rainfall rate estimates in an operational environment. They rely on the fact that as the radar pulse propagates through precipitation, the oblate raindrops introduce a larger phase delay in the horizontally polarized direction than in the vertical. Some advantages of this method are that the phase delay is more nearly proportional to the rain rate than is the reflectivity, the delay is unaffected by hail, and that the total differential phase delay along a path is a measure of the integrated rainfall. In this paper we analyse observations and explore the critical sensitivity of the differential phase shifts to assumed rain drop shapes.

## The Differential Phase Technique

The two-way specific differential phase shift, $K_{dp}$, in a given radar pulse volume is twice the real part of the difference between the two complex propagation constants $k_h$ (horizontal polarization) and $k_v$ (vertical) and is defined as (Oguchi, 1975),

$$K_{dp} = 2\mathrm{Re}(k_h - k_v) \quad m^{-1}$$

$$k_{h,v} = k_0 + \frac{2\pi}{k_0}\int_0^{D_{max}} f_{h,v}(D, \alpha(D))N(D)dD \quad m^{-1}$$

Both of these constants are simply $k_0$, $(2\pi/\lambda)$ the free space value, with a small additional term to account for the polarization dependent propagation properties caused by the presence of the precipitation in the pulse volume, where $f_{h,v}$ are the forward scattering amplitudes (defined by Oguchi (1983)), which are functions of drop size ($D$) and axial ratio, $\alpha(D)$. The function $\alpha(D)$ is often referred to as the drop-shapes model and this encapsulates the assumed relationship between size and drop-shape. We must also keep in mind that this is a propagation effect which produces cumulative phase shifts with range; forward scattering in the rain medium adds a small phase shift to the original incident radar pulse.

The definition above has SI units of (radians)$\cdot m^{-1}$. However a more practical definition would be $^\circ/km$. so a conversion factor is incorporated into the definition.

$$K_{dp} = 2\mathrm{Re}(k_h - k_v)\frac{180}{\pi}10^3 \quad ^\circ \cdot km^{-1}$$

[0] *Cost-75 International Seminar on Advanced Weather Radar Systems. Brussels. 20-23 September 1994. To be published in 1995*

Actual radar measurements must rely on estimating how the phase difference ($\phi_{dp} = \phi_v - \phi_h$) between the horizontally and vertically polarized returns varies with range. The Doppler width of the returned signal introduces an inherent random error in the $\phi_{dp}$ estimate, which is further amplified when the range derivative, $K_{dp}$, is computed. We must also consider that the measured value of $\phi_{dp}$ may be partially affected by *backscattered* differential phase shift, but fortunately this is rare for the relatively long wavelength we are considering ($9.75cm$).

Providing that we use only the sections of the radar beam that dwell in the rain, $K_{dp}$ potentially possesses the attribute of a nearly linear relationship with rain rate. If this could be established in an operational situation, some of the errors inherent in the use of a reflectivity($Z$)-rain rate relationship may be eliminated. Some of these errors are related to the incomplete knowledge of the distribution of different drop sizes in any given resolution cell of the radar beam. The heart of this problem lies in the fact that reflectivity measurements are proportional to $\sum D^6$ over some unit volume but rain rates are proportional to $\sum D^{3.63}$. This difference in the exponent implies that reflectivity-rain rate relationships are dependent on the details of the drop size distribution. Fitted model results in this research indicate that $K_{dp}$ appears to be approximately proportional to $\sum D^{4.75}$; this drastically reduces, but does not eliminate, the effects of variable drop size distributions.

In addition, $K_{dp}$ measurements should theoretically confer practical advantages over reflectivity measurements. The first of these is the elimination of absolute reflectivity calibration, as $K_{dp}$ is based on phase measurements which do not require external calibration. Secondly, the physical phenomenon we are exploiting is a propagation effect and so the total differential phase change naturally provides an integrated rainfall rate. Finally, the same propagation integration effect may be utilised to infer measurements in regions of heavy clutter if we assume that clutter-free gates can be identified on either side of the affected area. This technique also affords the possibilities of accurate rain rate measurements in the presence of hailstones. As hailstones are assumed to tumble randomly, they should not contribute to $K_{dp}$ estimates, which are exclusively affected by raindrops. Attenuation is not an issue, as long enough power is returned to make an actual phase measurement.

Of course, a few practical drawbacks also exist. Most crucially, at long wavelengths ($\geq 10\ cm$), the differential phase shift can be very small (for $R \leq 10mm/hr$) compared to the noise inherent in the phase estimation. $K_{dp}$ measurements are very sensitive to clutter in the beam but they can be identified and these gates ignored. The theory behind the $K_{dp}$-rain rate relationship is very different for rain and for ice or melting-layer regions and so these methods do not apply to ice precipitation.

### Drop-shape model effects on $K_{dp}$-$R$ relationship

In essence, all models for S-band $K_{dp}$-$R$ relationships combine either Mie or Rayleigh scattering theory modified to account for non-spherical scatterers, drop shapes, and some parameterized drop size distribution (DSD), along with terminal velocities as a function of drop size. In this section, we explore the sensitivity of a $K_{dp} - R$ relationship to the assumed drop shapes.

The precise shape of small drops is well known to have a large effect on differential reflectivity ($Z_{DR} = log_{10}\frac{Z_h}{Z_v}$) and the same issue affects $K_{dp}$, but has attracted little attention except for Tan et al (1991). Sachidananda and Zrnic (1986) in an initial model of a $K_{dp} - R$ relationship used Green's (1975) shapes and produced the relationship $K_{dp} = 0.03R^{1.15}$ for S-band measurements. Green's shapes are convenient for their analytic form but inaccuracies for small and large equivalent diameters introduce unacceptable errors for the purposes of interpreting polarization-diversity measurements. It has been shown that more spherical smaller drops ($D_{eq} < 2\ mm$) are needed to explain $Z_{DR}$ measurements (Goddard and Cherry, 1984) and $\rho_{hv}$ observations (Illingworth and Caylor, 1991) in light rain, and in heavy rain, more oblate large drops are needed as predicted by Beard and Chuang (1987) to agree with measured $Z_{DR}$ (Illingworth and Caylor, 1989).

The axial ratios in Table 1 were derived using the precise axial ratios of Beard and Chuang for drops with $D_{eq} > 2\ mm$ and assuming a straight line between the axial ratio of 0.928 at 2 $mm$ and the axial ratio of 1.000 at 1 $mm$, as the empirical results of Goddard and Cherry (1984) require and with perfectly spherical drops for $D_{eq} < 1\ mm$. We call these the "modified" Beard and Chuang (BC) drop shapes.

| $D_{eq}$ | Axial Ratio Modified BC (1987) | Axial Ratio Green (1975) |
|---|---|---|
| 0.5 | 1.000 | 0.994 |
| 1.0 | 1.000 | 0.976 |
| 2.0 | 0.928 | 0.917 |
| 3.0 | 0.853 | 0.843 |
| 4.0 | 0.778 | 0.769 |
| 5.0 | 0.708 | 0.701 |
| 6.0 | 0.642 | 0.639 |
| 7.0 | 0.581 | 0.585 |
| 8.0 | 0.521 | 0.537 |
| 9.0 | 0.466 | 0.495 |
| 10.0 | 0.411 | 0.457 |

Table 1: Modified Beard & Chuang (1987) and Green (1975) Drop Shapes

Using these drop shapes, the analytic terminal velocity function of Pruppacher and Klett (1980), with a Marshall-Palmer ($N_0 \exp(-\Lambda D_{eq})$) drop size distribution where $N_0 = 8000 mm^{-1} m^{-3}$, and varying the exponential slope to achieve different rain rates, the $K_{dp}$

values in Table 2 for the S-band wavelength of $9.75cm$ were computed using the Rayleigh-Gans scattering values. For contrast, the results of performing the same computations with Green's (1975) drop shapes are also presented. A parallel set of computations and comparisons were performed for a C-band wavelength of 5.35cm (Table 3) using a numerical (T-matrix) method to account for the Mie scattering by the larger drops. For both wavelengths, Green's shapes lead to differences of nearly a factor of 2 for the lowest rain rates.

| Rain rate $(mm/hr)$ | $K_{dp}(°/km)$ (Modified BC) | $K_{dp}(°/km)$ (Green) | Ratio |
|---|---|---|---|
| 0.86 | 0.0089 | 0.0203 | 2.28 |
| 1.55 | 0.0221 | 0.0417 | 1.89 |
| 2.41 | 0.0421 | 0.0709 | 1.69 |
| 3.04 | 0.0589 | 0.0942 | 1.60 |
| 5.02 | 0.1194 | 0.1735 | 1.45 |
| 8.78 | 0.2563 | 0.3424 | 1.34 |
| 16.43 | 0.5920 | 0.7359 | 1.24 |
| 33.61 | 1.5088 | 1.7662 | 1.17 |
| 50.16 | 2.5266 | 2.8827 | 1.14 |
| 77.50 | 4.4019 | 4.9079 | 1.11 |
| 124.72 | 8.0335 | 8.7760 | 1.09 |
| 210.64 | 15.4744 | 16.6022 | 1.07 |
| fit | $K_{dp} = 0.012R^{1.37}$ | $K_{dp} = 0.024R^{1.22}$ | |

Table 2: Model Predicted rain rates and S-band $K_{dp}$ along with fitted power law

| Rain rate $(mm/hr)$ | $K_{dp}(°/km)$ (Modified BC) | $K_{dp}(°/km)$ (Green) | Ratio |
|---|---|---|---|
| 0.86 | 0.023 | 0.056 | 2.45 |
| 1.55 | 0.054 | 0.106 | 1.96 |
| 2.41 | 0.100 | 0.173 | 1.72 |
| 3.04 | 0.139 | 0.225 | 1.62 |
| 5.02 | 0.276 | 0.401 | 1.45 |
| 8.78 | 0.580 | 0.769 | 1.33 |
| 16.43 | 1.315 | 1.617 | 1.23 |
| 33.61 | 3.288 | 3.805 | 1.16 |
| 50.16 | 5.437 | 6.142 | 1.13 |
| 77.50 | 9.319 | 10.308 | 1.11 |
| 124.72 | 16.636 | 18.077 | 1.09 |
| 210.64 | 31.115 | 33.275 | 1.07 |
| fit | $K_{dp} = 0.031R^{1.32}$ | $K_{dp} = 0.064R^{1.164}$ | |

Table 3: Model Predicted rain rates and C-band $K_{dp}$ along with fitted power law

Although we do not explore sensitivity to differing DSD forms such as gamma distributions, an investigation of rain rate as a function of DSD,

$$R = 0.6 \times 10^{-3}\pi \int_0^{D_{max}} w_t(D) D^3 N(D) dD \quad mm/hr$$

where $w_t(D)$ is some appropriate terminal velocity function and $N(D)$ represents the relevant DSD function (per unit volume), reveals that both rain rate and $K_{dp}$ are linearly proportional to the constant $N_0$ in the drop-size distribution. This implies that variations in $N_0$ should only change the constant in the power law ($K_{dp} = aR^b$) and not the exponent itself. One can also predict the change in this constant from the exponent. If we denote the original $N_0 = 8000 mm^{-1} m^{-3}$ as $N_{ref}$, the constant itself will change by $(\frac{N_0}{N_{ref}})^{b-1}$, so doubling the value of $N_0$ should change the constant in the power law by 30% (for $b = 1.37$), representing a reasonable degree of insensitivity. However, distributions with different overall shapes, i.e. different exponents in a gamma DSD, could lead to possibly significantly different power law relationships. Any function which weights the small (nearly spherical drops) less will lead to a smaller exponent as demonstrated theoretically by Tan et al (1991).

## Model Comparison with Data

To compare model drop sizes with observations, we employed the Rutherford-Appleton Laboratory's Chilbolton S-band research radar which operates at the $9.75cm$ wavelength with a $0.28°$ $3dB$ beamwidth. The $0.5$ $\mu$sec pulse produces a $75m$ resolution volume in range and the digital hardware gates the return echo at the same resolution. For a fuller description of the detailed arrangements see Eastment and Illingworth (1994).

Figures 1 and 2 show reflectivity and $K_{dp}$ data taken from a single PPI scan in azimuth (a horizontal section) at an elevation of $1.5°$ on 7 Sept. 1993. On this day, a band of heavy rain in the English Channel was moving north-east and over the Chilbolton radar. This scan across the south intercepted some fairly high (35-45 dBZ), widespread reflectivities with one small core ($\approx$ 0.5km across) of 50 dBZ. The $K_{dp}$ estimates in Figure 2 represent averaging of very large samples. Specific differential phase shift estimates have been computed using the difference of adjacent mean values of $\phi_{dp}$ at 32 consecutive gates, thus producing a $K_{dp}$ estimate at 2.4km intervals in range. This estimate was additionally averaged for 10 $s$ in azimuth to produce the blocks with 2.4km by $10°$ dimensions. These $K_{dp}$ estimates were very tightly restricted to very high values of $\rho_{hv}$ ($> 0.9$) to ensure that only rain and not ground clutter or melting layer estimates were being considered.

In Figure 3, the $R$ values and $K_{dp}$ estimates have been taken from Figure 1 and 2, with the same 2.4km range resolution but without the azimuthal averaging for $K_{dp}$. The $R$ values have been derived using a standard $Z = 200R^{1.6}$ (see Battan (1973)) conversion at each gate. The values of $K_{dp}$ have been sorted into rain rate bins, with each point and error bar representing the mean value and standard error of $K_{dp}$ for each $1mm/hr$ wide bin. For comparison, the relations predicted with the use of modified BC shapes and by Green's shapes are also plotted, as are the results of Sachidananda and Zrnic (1987).

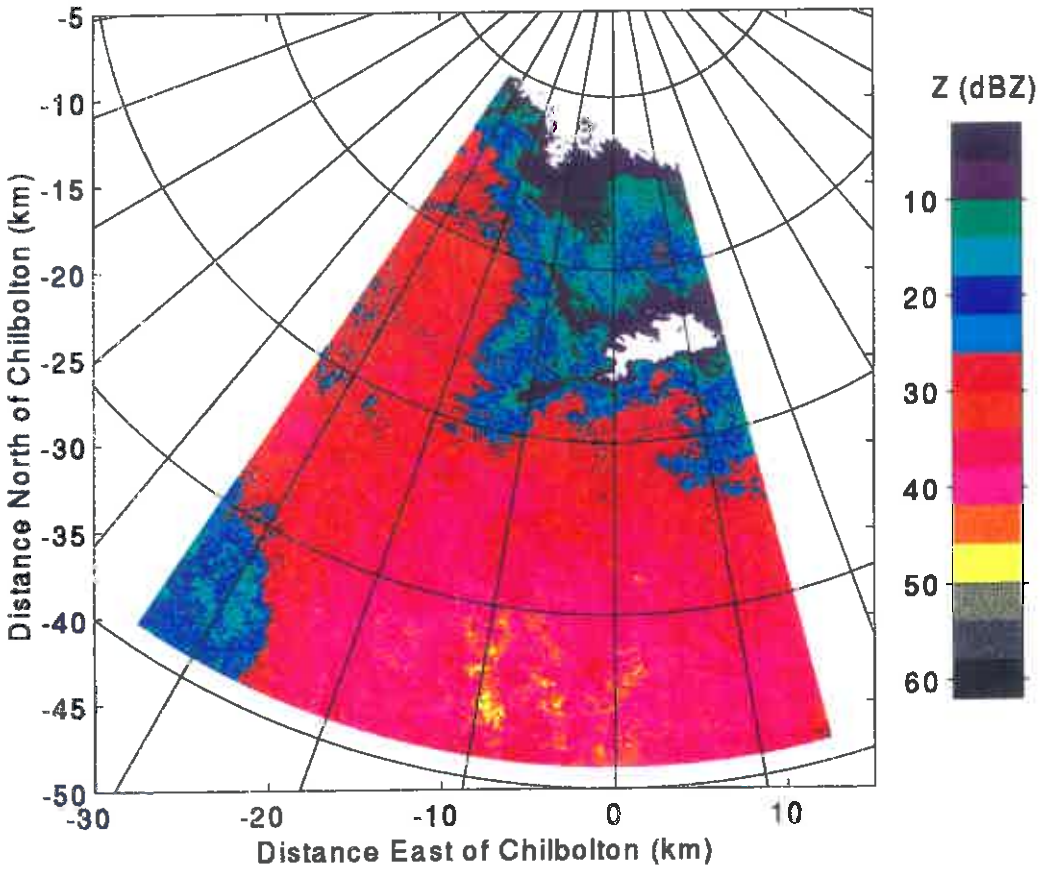


Figure 1: Reflectivity Map from the PPI (azimuthal) scan at 17:23:10 GMT, 7/9/1993

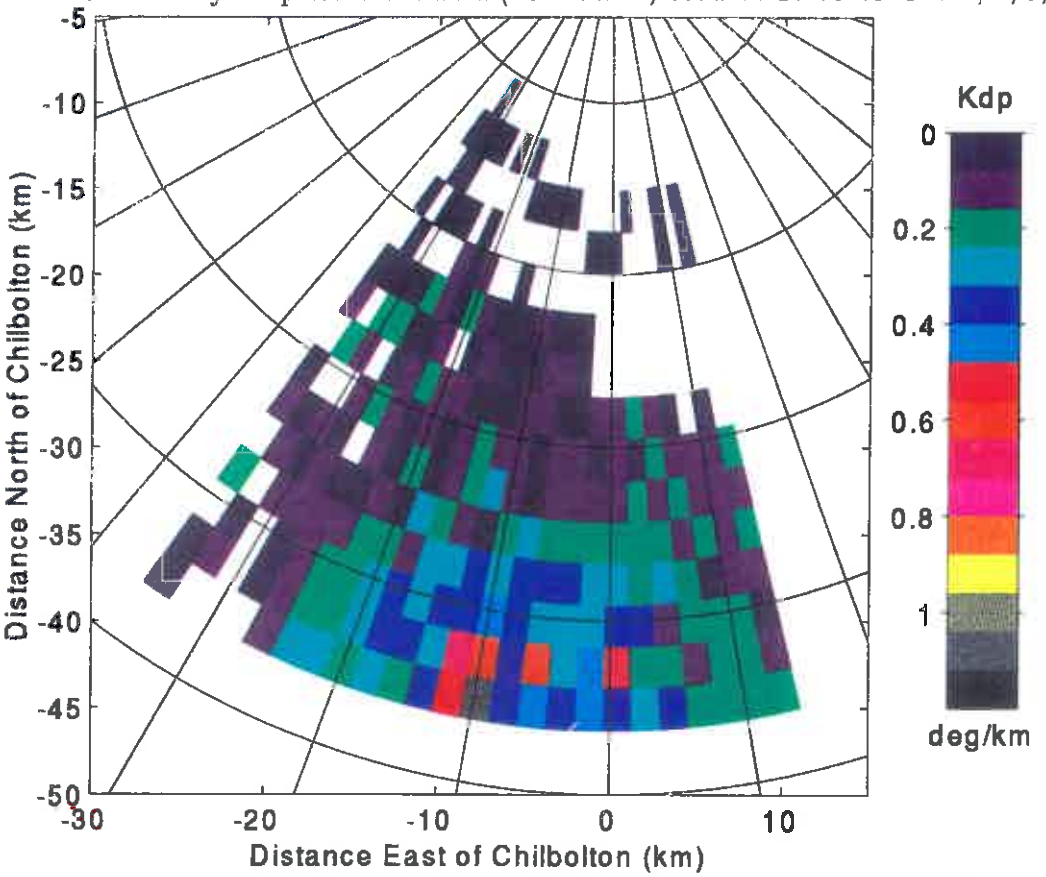


Figure 2: $K_{dp}$ Estimates Map from the PPI (azimuthal) scan at 17:23:10 GMT, 7/9/1993

For the range of low rain rates with small error bars (0-15 mm/hr), these data agree far more closely with the predictions of the model using modified BC shapes than with the Green's shape predictions, and confirm that Green's drop shapes with their non-spherical small drops ($D_{eq} < 1mm$) are inappropriate for polarization-diversity radar estimates of rainfall.

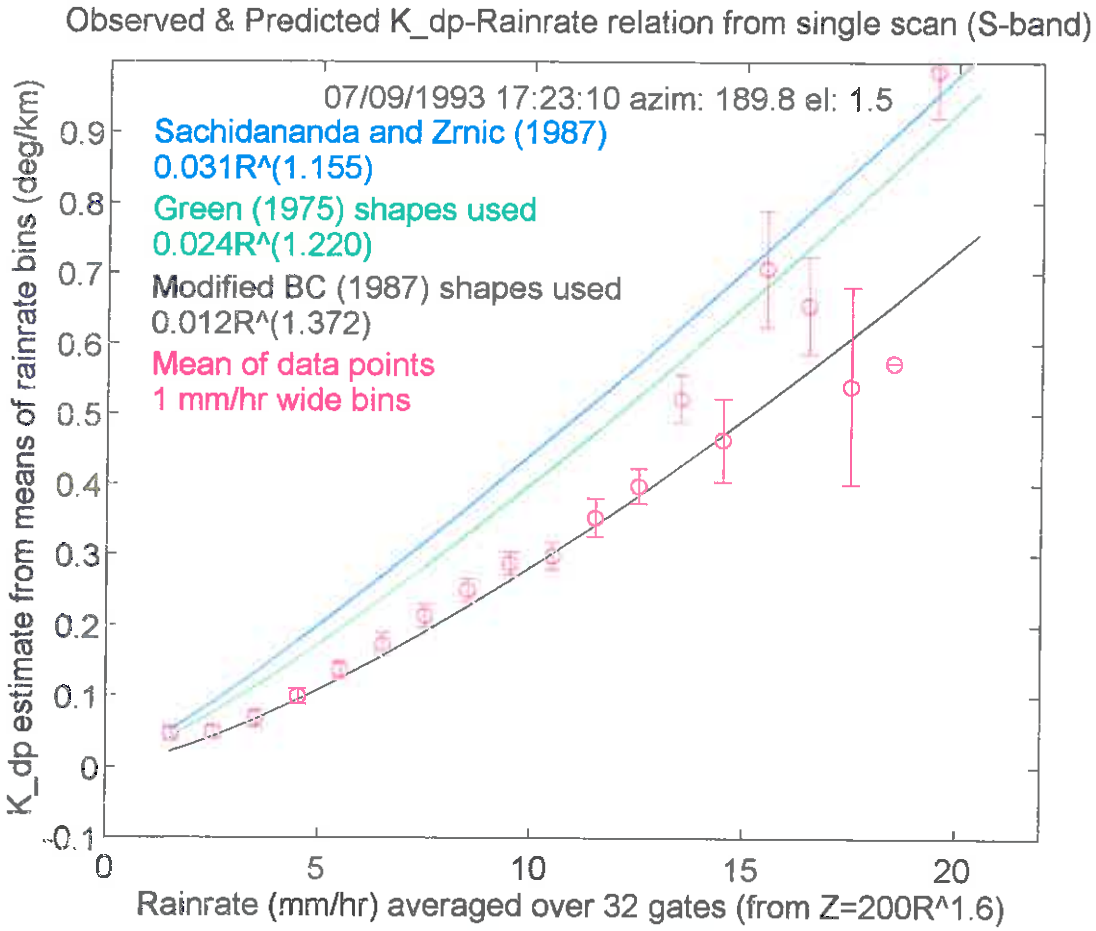


Figure 3: $K_{dp}$ estimates vs. Rain rate estimates (from Z)

### Path Integrated Rainfall Rates

Although serious signal to noise problems plague the measurement of $K_{dp}$ for low rain rates, the physically intrinsic integration of the propagation may allow us to estimate mean rain rates over long stretches of low rain rates. Essentially, we are assuming that

$$\int_{r_1}^{r_2} R dr/\Delta r \approx \left[(\int_{r_1}^{r_2} K_{dp} dr)/(a\Delta r)\right]^{1/b} = \left[\frac{\phi_{dp}(r_2) - \phi_{dp}(r_1)}{a\Delta r}\right]^{1/b}$$

where $a$ and $b$ are the constants in the power law $K_{dp} = aR^b$ and $r_1, r_2$ refer to two widely separated range points along the radar beam. The above approximation is exactly true when the rainfall rate is constant with range or the exponent $b$ is unity. We must, however, consider how deviations from rainfall uniformity affect the approximation. If we imagine two stretches of rainfall with the same $\overline{R}$, but differing spatial distributions, we can begin to decide how useful this approximation is. In the first case we use a uniform distribution so that $R(r) = \overline{R}$ between our two radar gates, $r_1$ and $r_2$, and $K_{dp}$ measurements will yield exactly the true $\overline{R}$, assuming the power law relationship is valid. In the second case, using a distribution with $R(r) = 10\overline{R}$, but extending only $1/10$ of the distance between $r_1$ and $r_2$, the $K_{dp}$ estimate yields $\hat{R} = 10^{(1-\frac{1}{b})}\overline{R}$. For $b = 1.37$, the predicted and observed exponent, this amounts to an 86% overestimate of the path integrated rainfall over the distance $r_2 - r_1$ for this particular case. The critical parameter is clearly the exponent in the power law. As $b$ approaches 1, then the overestimation vanishes. The predicted exponent at C-band is 1.32 and the overestimate with this extreme distribution comes down to 73%.

Figure 4 illustrates this integration effect with a plot of $\phi_{dp}$ vs. range for a single ray with the indicated azimuth and elevation (0.5°). Although there is clearly structure present in this diagram, notably the steep slopes (high $K_{dp}$ and rain rate) at 54 $km$ and 67 $km$ range, the difference between the phase at the starting point, $\phi_{dp}(r_1) \approx -20°$ at 35 $km$, and the phase at the end point, $\phi_{dp}(r_2) \approx -6°$ at 70 $km$ yields an estimate of mean rain rate ($\overline{R}$) between these two points of 13 $mm/hr$ using $a = 0.012$ and $b = 1.372$ from Table 2. Although the $Z$ estimate of mean rain rate between these two points produces a lower estimate of mean rain rate ($8mm/hr$), this is in line with the predicted biases of the $R - K_{dp}$ relation when employed over long distances.

This integrated rain rate estimate only required $\phi_{dp}$ measurements at two clutter-free range gates, without the need for any radar data over the intervening distance. Thus even severe ground clutter preventing any radar observations between these two gates would not affect this estimate of the rainfall.

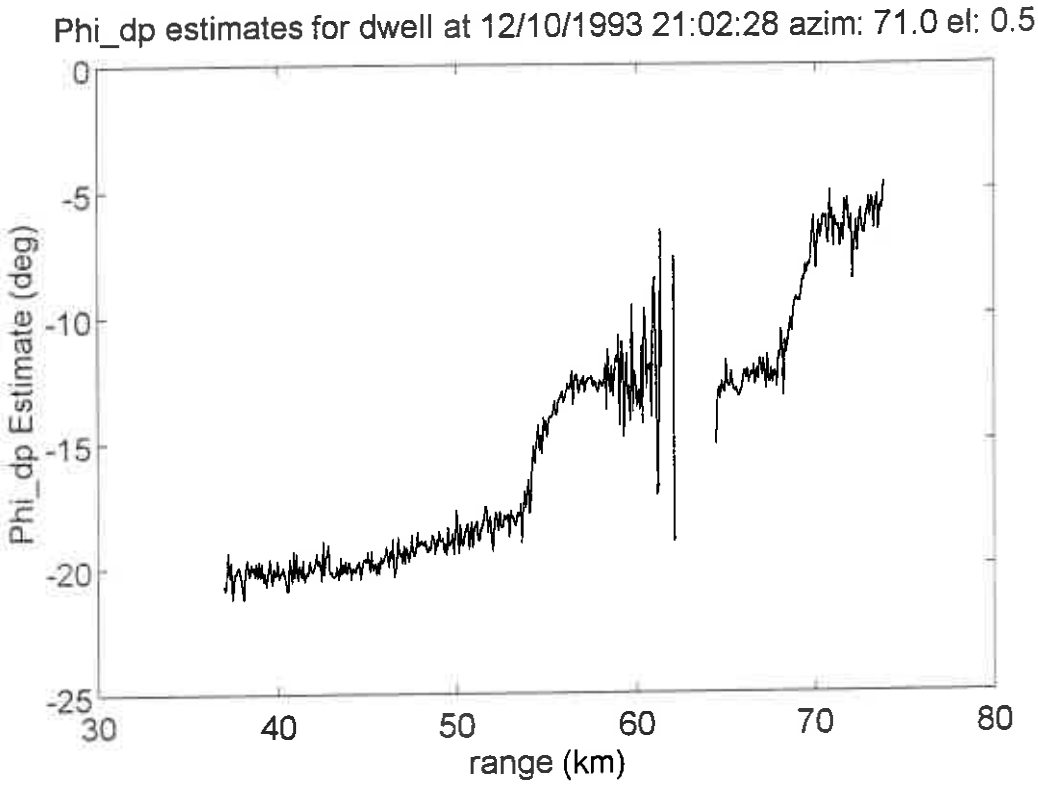


Figure 4: Integration Effect in $\phi_{dp}$ Measurements

## Conclusions

There is a very clear sensitivity to drop shapes (and thus drop size distributions) in the $R - K_{dp}$ relationships, as these observations and the theoretical study of Tan et al (1991) demonstrate, and we believe that the modified BC shapes presented are the most appropriate shapes on the basis of the results of Goddard and Cherry (1984) and Illingworth and Caylor (1989), and the observations presented in this paper.

This drop shape model leads to the relationship $K_{dp} = 0.012R^{1.37}$ for a Marshall-Palmer distribution, and the data for low rain rates confirm this at S-band: at C-band the same model predicts $K_{dp} = 0.031^{1.321}$. This relationship, with the relatively small exponent, should be reasonably insensitive to changes in $N_0$. The integration properties of $\phi_{dp}$ measurements are moderately well preserved for extreme cases of non-uniform rainfall (compared to Z-estimates over the same distance) at S-band and C-band. We have not attempted to consider the errors associated with estimating $K_{dp}$ values as we are only proposing a revision of the $K_{dp} - R$ relationship model of Sachidananda and Zrnic (1986) and suggesting further empirical work should be undertaken to validate this revision. The host of practical advantages of specific differential phase shift estimates of rain rate suggest it is most beneficial when used in combination with $Z$ rather than as a replacement.

## Acknowledgements

Dopplerisation of the Chilbolton radar was carried out under NERC grant GR3/7618 and this analysis was supported by grants GST/02/718 and CEC environment program EV5V-CT92-0182. We thank our colleagues at RAL (RCRU) and at the JCMM for useful advice and invaluable engineering support.

## References

Battan (1973) *Radar Observations of the Atmosphere*. University of Chicago Press, Chicago.

Beard K. V. and Chuang C. (1987) A New Model for the Equilibrium Shape of Raindrops. *J. Atmos. Sci.* **44**, 1509-1524.

Eastment J. D. and Illingworth A. J. (1994) A hardware implementation of LDR and Doppler Measurements. *These Proceedings.*

Goddard J. W. F. and Cherry S. M. (1984) The ability of dual-polarization radar (copolar linear) to predict rainfall rate and microwave attenuation. *Radio Sci.* **19**, 201-208.

Green A. W. (1975) An Approximation for the Shapes of Large Raindrops. *J. Appl. Meteorol.* **14**(December), 1578-1583.

Illingworth A. J. and Caylor I. J. (1989) Polarization Radar Estimates of Raindrop Size Spectra and Rainfall Rates. *J. Atmos. Ocean. Technol.* **6**, 939-949.

Illingworth A. J. and Caylor I. J. (1991) Co-polar Correlation Measurements of Precipitation. *Prepr., Radar Meteorol. Conf.* **25th**, 650-653.

Oguchi T. (1975) Rain depolarization studies at centimeter and millimeter wavelengths: Theory and measurement. *J. Radio Res. Labs. Japan* **22**, 165-211.

Oguchi T. (1983) Electromagnetic wave propagation and scattering in rain and other hydrometeors. *Proc. IEEE* **71**, 1029-1078.

Pruppacher H. R. and Klett J. D. (1980) *Microphysics of Clouds and Precipitation. 2nd ed.* D. Reidel, Dordrecht, Holland.

Sachidananda M. and Zrnic D. S. (1986) Differential propagation phase shift and rainfall estimation. *Radio Sci.* **21**, 235-247.

Sachidananda M. and Zrnic D. S. (1987) Rain Rate estimates from Differential Polarization Measurements. *J. Atmos. Ocean. Technol.* **4**, 588-598.

Tan J., Bebbington D. H. O., and Holt A. R. (1991) Theoretical Studies of Differential Propagation Phase Shift in Meteorological Polarization Diversity Radars at Centimeter Wavelengths. *Proceedings. 7th International Conference on Antennas and Propagation. IEE conference publication.*

# THE USE OF DOPPLER AND POLARISATION DATA TO IDENTIFY GROUND CLUTTER AND ANAPROP.

D R Wilson (JCMM, U of Reading, UK, RG6 2AU;FAX 44 734 352604)
A J Illingworth and T M Blackman.

## 1. INTRODUCTION

Ground clutter can be a major problem for the quantitative measurement of precipitation by radar. Large errors in rainfall estimates can arise if the high power radar returns from ground reflections are interpreted as precipitation. Two approaches have been proposed to overcome this problem. One method is to identify and reject those gates which are affected by clutter and then substitute values of reflectivity which are interpolated from neighbouring uncontaminated gates. In its simplest form a constant 'clutter map' can be used based on observations made on dry days. However clutter, and especially the returns due to anomalous propagation, vary from day to day, and so it is better to derive a 'dynamic' clutter map for each radar scan. A second, more powerful method, available only for Dopplerised radars, relies on identifying clutter by its zero mean velocity and narrow Doppler width; real time filtering can be used to reject the component of the clutter and recover the precipitation echo.

In this paper we will investigate methods of identifying cluttered gates for a radar which does not have a Doppler capability. For the purposes of validating these non-Doppler techniques, we will use the observed Doppler spectrum to separate out the components of the return due to clutter and precipitation and this will constitute the 'truth' for testing the algorithm. An example is shown in Figure 1 where the return from the precipitation with a velocity of about 5m/s can be clearly distinguished from the stationary ground clutter. In previous work, there has been a tendency to display plausible maps of precipitation fields before and after clutter removal, but without an independent means of knowing if all the clutter has been identified.

We shall first examine the efficiency of non-Doppler methods which rely on the statistical properties of the fluctuating power recorded by successive radar pulses at each gate. The basis of these techniques is that the precipitation targets are continually reshuffling in space and should produce a fluctuating echo with a standard deviation equal to the mean value, whereas clutter is relatively stationary and the return varies only slowly with time. Tatehira and Shimizu (1978) show that, in theory, the ratio of the mean power to the standard deviation of the amplitude should be a unique function of the ratio of the clutter to the precipitation power. This suggests a non-Doppler method of measuring the precipitation return in the presence of clutter.

In this paper we will also explore the use of the linear depolarisation ratio (LDR) for identifying clutter. LDR is defined as the ratio of the cross-polar (e.g. vertically polarised) return to the co-polar (e.g.horizontally polarised) echo. We have not considered polarisation methods which use differential reflectivity (Hall et al, 1984, and Giuli et al, 1991), or values of co-polar correlation (Caylor and Illingworth et al, 1991) because with such techniques require pulse to pulse switching of the transmitted radiation. For ease of implementation we have also excluded methods which rely on recognising spatial patterns. The LDR technique has the advantage that it is relatively easy to implement (Eastment and Illingworth, 1994) and only requires the installation of a low power receive switch and an additional receiver chain.

*Cost-75 International Seminar on Advanced Weather Radar Systems*
*Brussels, 20-23 September 1994*
*To be published in 1995*

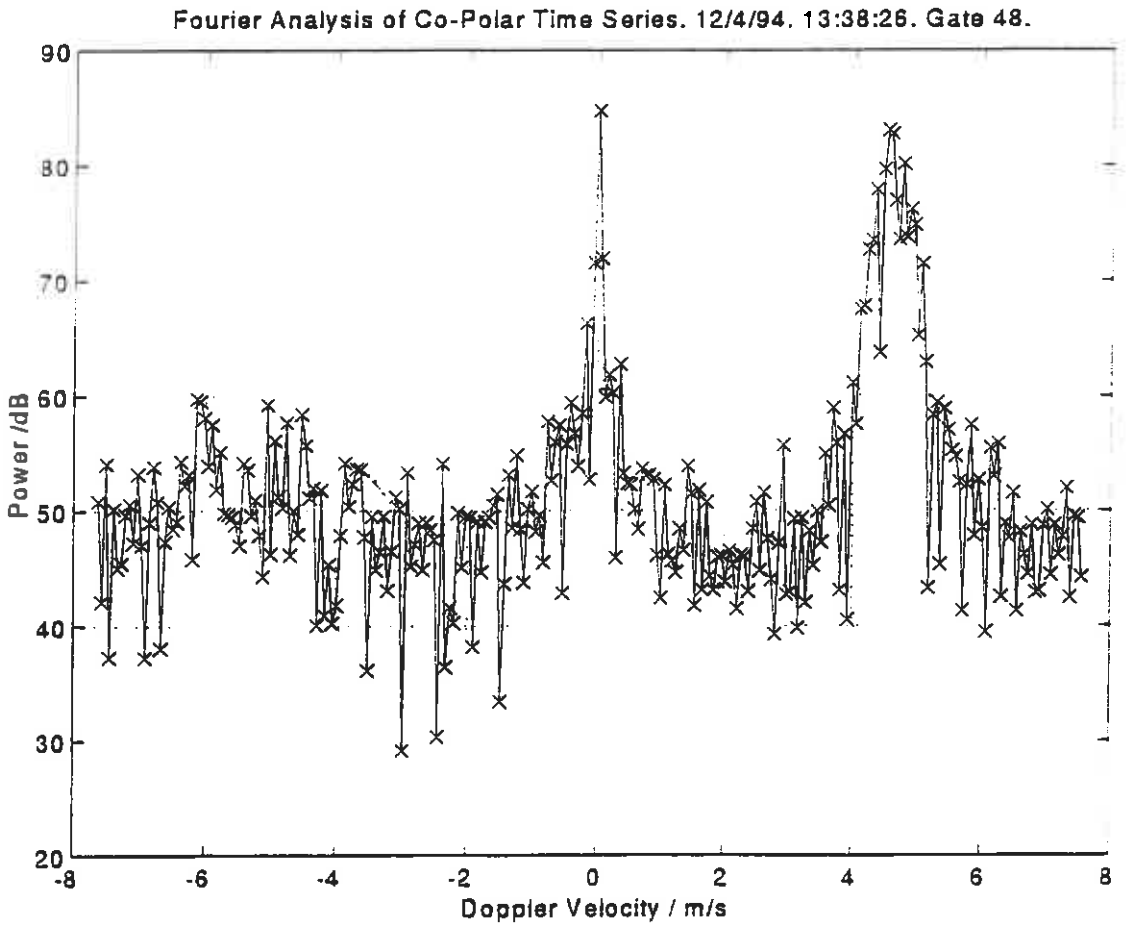


Figure 1. The Doppler spectrum of a gate showing both precipitation and ground clutter. The precipitation is the broad signal at about 5 m/s whereas the clutter has a narrow but non zero width centred around 0 m/s. By filtering this spectrum one can proportion power between precipitation and ground clutter and hence produce a 'truth' for later comparison.

## 2. DESCRIPTION OF THE RADAR MEASUREMENTS.

The observations described in this paper are taken with the DRAL Chilbolton which has both Doppler and polarisation diversity (Eastment and Illingworth, 1994). The radar operates at S-band (10cm wavelength) with a pulse repetition frequency of 305Hz (equivalent to a time delay of 3.28ms) between pulses of the same polarization, with the horizontally and vertically polarized pulses transmitted alternately. In this work we only consider the horizontally transmitted pulses and analyse the time series which are usually of 64 such pulses (210ms in total) and the ratio of the vertically to the horizontally polarised return (LDR). Most of the data presented is derived from vertical and horizontal sections through precipitation ; the quarter second dwell times leading to uncertainties in Z of about 1dB. Spectral analysis (e.g figure 1) demonstrates that the ratio of clutter to precipitation power for this data set varies from -30dB for pure precipitation to +30dB for heavily cluttered gates. The radar has a very narrow beam of 0.25 degrees width and low sidelobes. The absence of large hills means that most of the clutter is at a range of less than 20km.

## 3. THE DECORRELATION TIME OF THE POWER TIME SERIES.

The return echo fluctuates as the hydrometeors reshuffle, the decorrelation time being a measure of the Doppler width of the target. Precipitation should have much shorter decorrelation times than clutter. In an ideal case of truly stationary clutter the radar return is constant in time, but in reality clutter usually exhibits some degree of motion, especially if the target is trees or vegetation moving in the wind.

First considerations would suggest that a way of identifying clutter from precipitation would be to look at the decorrelation time of the power series, but Figure 2 reveals that the situation is rather more complicated. The decorrelation time ($\tau$) was derived from the time lag for the autocorrelation to fall below 1/e. The value of $\tau$ was recorded as an integral number of pulses; no attempt was made to extrapolate the data and any subsequent rises above the value of 1/e were ignored. The estimated ratio of the clutter to precipitation power for each gate was computed from the Doppler spectrum.

The data for Figure 2 indicate that high decorrelation times are not an effective means of identifying clutter. Firstly, the finite width of the Doppler spectrum of the clutter means that it does not have excessively large decorrelation times; secondly, it is possible to obtain reasonably long decorrelation times even for precipitation. In addition medium levels of clutter, when the ratio of the clutter to the precipitation is less than 10dB, can have a very high effective Doppler width and a very low decorrelation time; Figure 1 is an example of a spectra with a low value of $\tau$. Low signal to noise ratios can affect $\tau$; for S/N above 10dB the effect is small, but when S/N falls below 5dB then $\tau$ rapidly falls to one inter-pulse delay. Clutter and precipitation usually have large S/N ratios so this is not generally a practical problem.

One conclusion is that, contrary to expectations, very short decorrelation times (less than on inter-pulse delay of 3.3ms) are efficient indicators of medium levels of clutter.

## 4. STATISTICAL ESTIMATORS OF CLUTTER FROM THE POWER TIME SERIES.

Theoretical prediction by Tatehira and Shimizu (1978) suggest that the ratio of the mean power to the variance of the amplitude of the time series can be used to derive the ratio of clutter to precipitation power. To test this hypothesis the data for both cluttered and uncluttered gates are plotted in Figure 3 and compared with the theoretical relationship predicted by Tatehira and Shimizu.

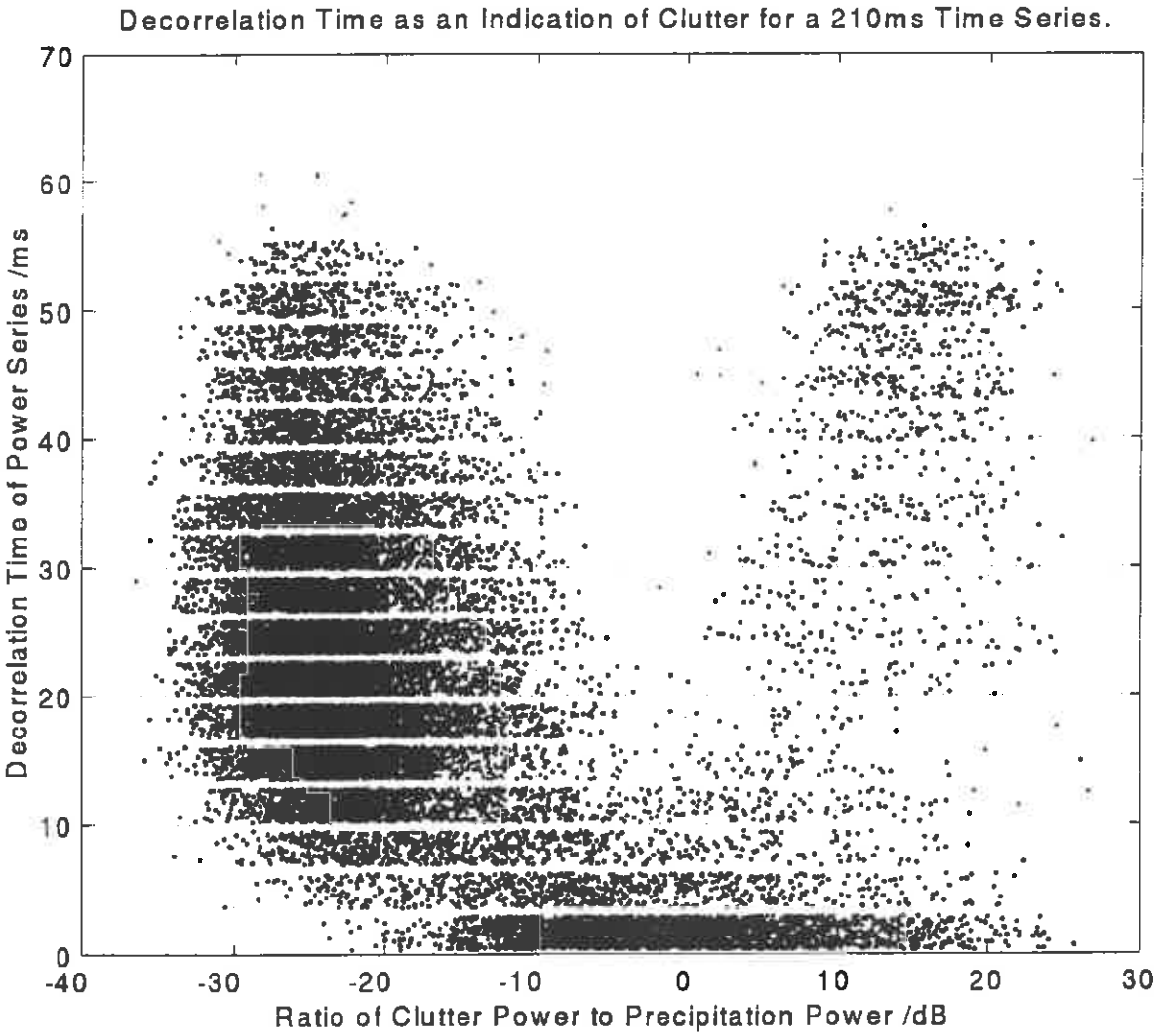


Figure 2. The decorrelation time of the power time series against the amount of clutter identified by filtering the Doppler spectrum. Since each measurement produces a half integer decorrelation time (in pulses) a small random value has been added or subtracted from each decorrelation time in order to display the density of points on this plot.

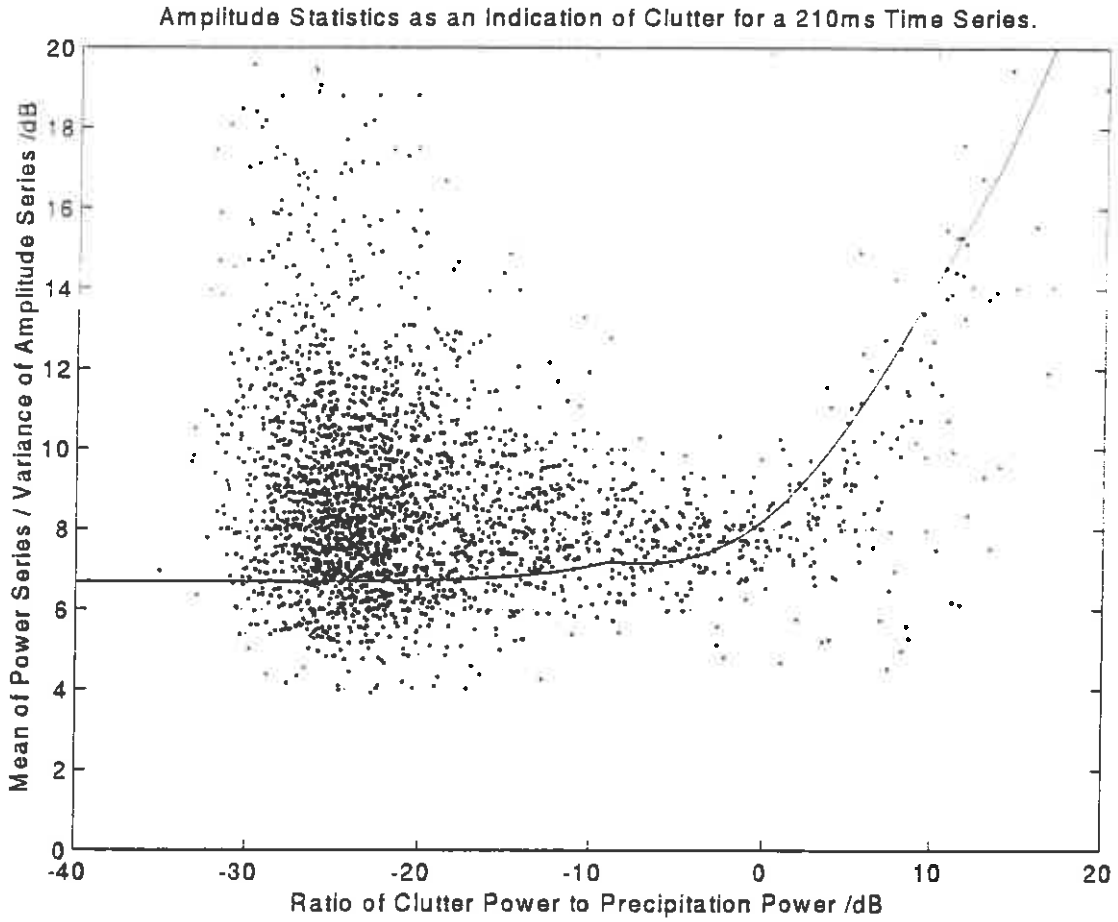


Figure 3. The performance of the statistical estimator at identifying clutter. The points show the ratio of the mean power to the variance of the amplitude series, the solid line gives the theoretical relationship for completely stationary clutter and a long averaging time. The points do not show quantitative agreement with the line.

The data in Figure 3 show poor agreement with theory. The ratio of the mean power to the variance is higher than it is expected to be in uncluttered precipitation; this is because each time series is not long enough to obtain an unbiased estimate of the variance. A longer time series will reduce this offset from the theoretical line but would lead to unacceptably slow scanning rates for the radar. However, the most serious error is in the points affected by clutter. Because the clutter is not totally stationary, the variance is significantly higher than expected, and so the data fall below the theoretical curve.

It is therefore concluded that the variance technique is not a reliable method for obtaining values of uncluttered Z in the presence of clutter. Even its application for identifying cluttered gates appears very limited.

## 5. THE LINEAR DEPOLARISATION RATIO.

The value of the cross polar return from precipitation is low. Theory and observations (Illingworth and Frost, 1991) confirm that the highest values of LDR for a radar observing precipitation at low elevation is about -13dB. These values are found in the bright band, and are caused by wet oblate melting snowflakes which tumble as they fall. Initial examination of ground clutter reveals that LDR values are much higher than those found in precipitation and this suggests a simple LDR criterion for identifying clutter.

Analysis of the data set (Figure 4) reveals that this LDR technique can occasionally be ambiguous. The theoretical curve is based on the assumption that clutter has an LDR of zero dB and precipitation a value of minus infinity, equivalent to zero cross-polar return. The vast majority of the precipitation in figure 4 does have an LDR value below -15dB, but the difficulty is that the LDR value of clutter is not zero. There is a tendency for the LDR value of the more heavily cluttered gates to fall, evidently such clutter targets start to appear more spherical and do not reflect isotropically.

Initial expectations that it might be possible to use the value of LDR at a particular gate to subtract the clutter power from that gate are thus dashed; this is due almost entirely to the non-isotropic scattering of the clutter. Therefore the use of LDR is confined to identification purposes only, and not correction. Additionally, any threshold technique should not remove the melting layer from the data. Our data show that a threshold of -13dB is in fact a good estimator of whether a point is cluttered or not and correctly identifies 85% or cluttered points. An LDR of below -13dB indicates precipitation; 89% of gates containing precipitation are correctly categorised (Figure 4). This threshold should be incorporated into an overall detection algorithm; however it does not remove all the clutter points so it should be used in combination with other techniques.

## 6. THE COMBINED DETECTION ALGORITHM.

The overall detection algorithm suggested by the data is to flag clutter all those points where LDR is greater than -13dB and in addition to flag those where the decorrelation time is less than one pulse (3.3ms). This removes over 91% of the cluttered points but retains 88% of the uncluttered points without removing a large area of the melting layer.

Figure 5 demonstrates the effectiveness of the combined algorithm for a vertical profile where clutter exists at low elevations. Note that it is impossible from the Z values alone in the first three columns to identify the clutter with any degree of certainty. The fourth column shows the 'true' ratio of clutter to precipitation derived from the Doppler spectrum.

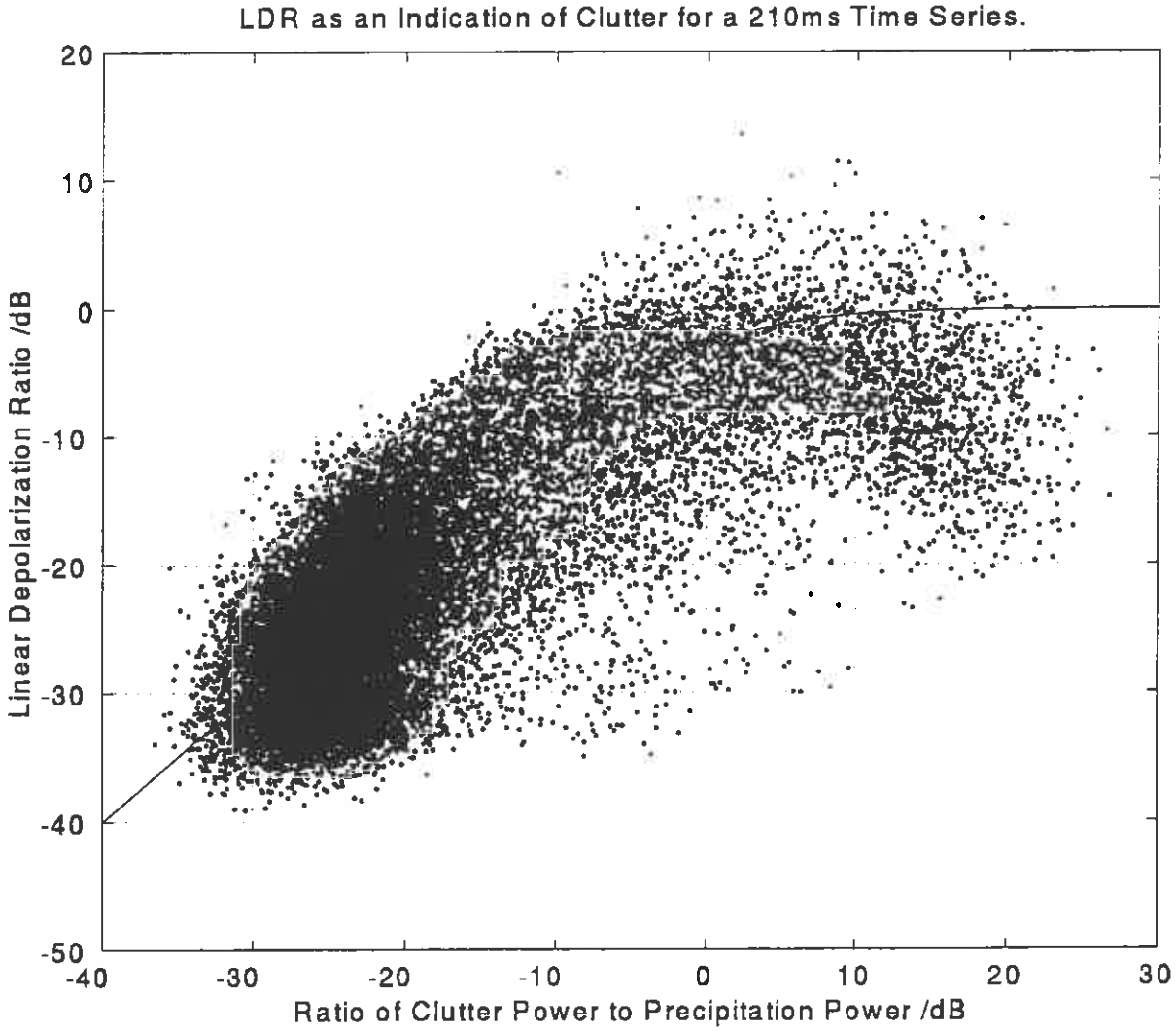


Figure 4. The Linear Depolarization Ratio of the unfiltered time series against the amount of clutter identified by filtering the Doppler spectrum. The points show individual measured values and the solid line is the theoretical relationship which should be followed if clutter reflects equally in both polarizations.

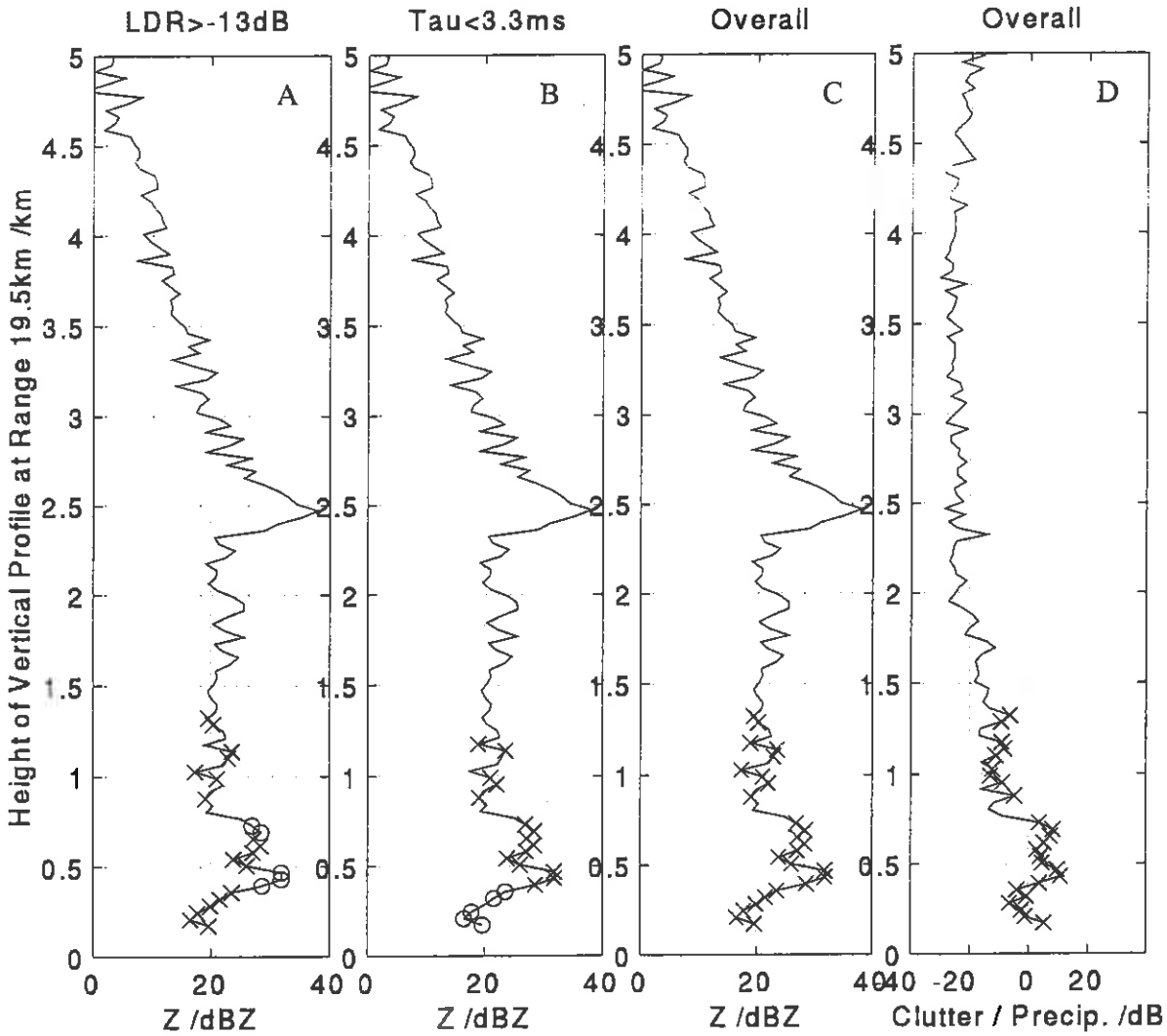


Figure 5. The effectiveness of the clutter identification algorithm on a vertical profile. The crosses 'x' mark those points identified by the algorithm as clutter. The circles 'o' mark those points which are actually affected by clutter to an extent that the reflectivity is increased by greater than 1dB and are not identified by the algorithm.

A) The solid line shows the profile of Z. The marked points are using LDR greater than -13dB to identify clutter. Some cluttered points are missed by the algorithm.

B) As in A but the marked points are only using the decorrelation time smaller than 3.3ms to identify clutter. Again, some cluttered points are missed.

C) As in A but using the decorrelation time smaller than 3.3ms or LDR greater than -13dB to identify clutter. No clutter points are missed.

D) The solid line shows the amount of clutter actually present. The marked points are as in C.

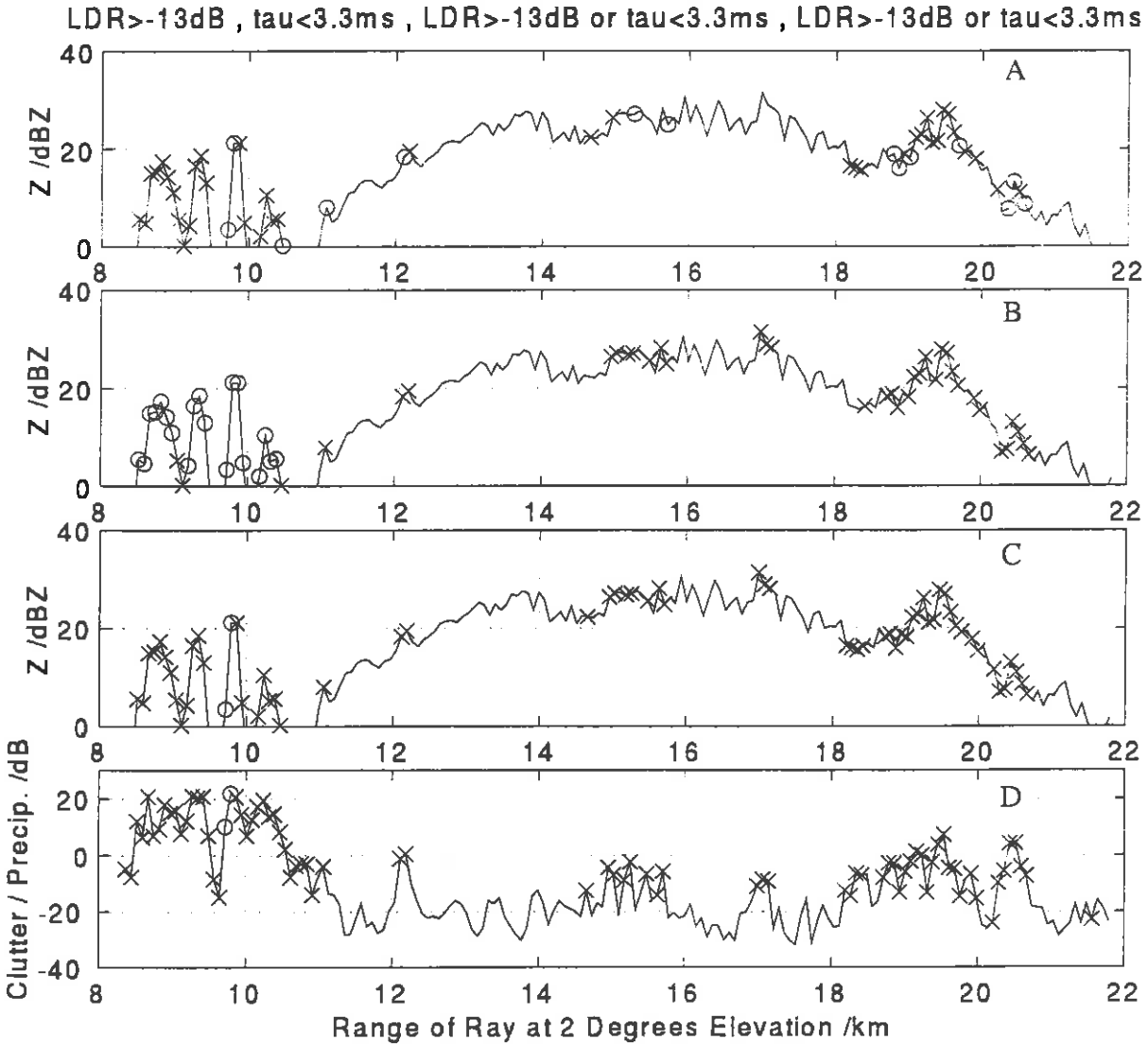


Figure 6. The effectiveness of the clutter identification algorithm on a ray.
The crosses 'x' mark those points identified by the algorithm as clutter.
The circles 'o' mark those points which are actually affected by clutter to an extent that the reflectivity is increased by greater than 1dB and are not identified by the algorithm.

A) The solid line shows the pattern of Z. The marked points are using LDR greater than -13dB to identify clutter. Some cluttered points are missed by the algorithm.

B) As in A but the marked points are only using the decorrelation time smaller than 3.3ms to identify clutter. Again, some cluttered points are missed.

C) As in A but using the decorrelation time smaller than 3.3ms or LDR greater than -13dB to identify clutter. Only two clutter points are missed.

D) The solid line shows the amount of clutter actually present. The marked points are as in C.

The crosses are points identified at ground clutter, the circles where ground clutter has not been recognised. The first column shows that LDR alone fails to locate all the clutter, whilst second column confirms that the decorrelation time also fails to identify some clutter points. However the third column confirms that the combined algorithm identifies all the clutter. Figure 6 shows a ray from the same scan with extensive clutter at ranges below 12km and again close to 20km. The figure again shows the success of the combined algorithm at eliminating clutter points but the failure of either part when considered on its own.

## 7. CONCLUSIONS.

Several methods of the identification of clutter by non-Doppler techniques have been suggested and their performances evaluated in the case where precipitation is corrupted by clutter. The full Doppler spectrum measured by the Chilbolton radar has been used to obtain the ratio of clutter to precipitation power at each gate to validate the non-Doppler techniques. The data suggest that short values of the decorrelation time are effective at picking out medium levels of clutter where the clutter power is similar to the precipitation power, but that this method fails for more heavily cluttered gates. The statistical fluctuations of the signal are not a good indicator of clutter in the case of mixed clutter and precipitation and should not be used to identify clutter on an individual gate basis. No non-Doppler technique investigated allows the clutter to be filtered out to give an uncluttered precipitation power. It is suggested that an effective way to remove clutter is to flag points with LDR values above -13dB or decorrelation times below one pulse (3.3ms). The measurement of decorrelation time can be performed without the recording of the complete time series by electronic processors so making the technique simple to implement.

## 8. ACKNOWLEDGEMENTS

This work was carried out with the support of NERC grant GR3/8523. We would like to thank colleagues at RCRU (DRAL) and JCMM for their contribution to the work reported here.

## 9. REFERENCES

Caylor I J and Illingworth A J (1991) 'Polarisation radar estimates of rainfall: Correction of errors due to the bright band and to anomalous propagation' in International Weather Radar Networking Cost 73 Final Seminar, pub Kluwer, Dordrecht.

Eastment J D and Illingworth A J (1994) A hardware implementation of LDR and Doppler measurements. These proceedings.

Frost I R, Goddard J W F and Illingworth A J (1991) Hydrometeor identification using cross polar radar measurements and aircraft verification. 25th Int Conf on Radar Met, Amer Meteorol. Soc, Boston p658-661.

Giuli D, Gherardelli, M, Freni A, Seliga T A and Aydin K. (1991) 'Rainfall and clutter discrimination by means of dual linear polarisation radar measurements. J Atmos and Ocean Technol, 8, Dec.

Hall M P M, Goddard J W F and Cherry S M (1984) Identification of hydrometeors and other targets by dual-polarisation radar. Radio Sci, **19**, 132-140.

Tatehira K and Shimizu T (1978) 'Intensity measurement of precipitation echo superposed on ground clutter - A new automatic technique for ground clutter rejection'. 18th Int Conf on Radar Met, Amer.Meteorol.Soc., Boston, pp 364-369.

# A HARDWARE IMPLEMENTATION OF LDR AND DOPPLER MEASUREMENTS

by J D Eastment (RCRU, RAL, U.K. FAX:+44 235 446140)
and A J Illingworth (JCMM, U.K. FAX: +44 734 352604)

## 1. Introduction

This paper describes the implementation of a linear de-polarisation ratio (LDR = 10 log [$Z_{CROSS}/Z_{CO}$] ) and Doppler capability on the Chilbolton 3 GHz radar [1], located near Winchester in Southern England and operated by the Radio Communication Research Unit of the Rutherford Appleton Laboratory. The specification of the radar is shown in Table 1. Approximate costings for upgrading magnetron-based reflectivity-only radars are presented, and some examples of LDR and Doppler data taken with the Chilbolton radar are briefly discussed.

## 2. Applications of LDR:

LDR is an excellent indicator of the presence of a melting layer, and as such, may be used to correct for the over-estimation of rain-rates derived from co-polar reflectivity data alone [2]. This makes it an attractive addition to networked radars, which commonly measure only Z. Other uses of LDR are in identification of radar returns from local ground clutter, and from distant clutter due to anaprop. In research radars, LDR may be combined with other measured parameters to determine particle phase, shape and fall mode.

## 3. Generalised implementation of LDR:

The simplest implementation of LDR for the case of a radar transmitting a single linear polarisation is shown in Figure 1. This assumes that the radar antenna has sufficient cross-polar discrimination (>20 dB), as this sets a lower limit on the measurable range of LDR. The PIN diode switch state is toggled from pulse to pulse, so that the receiver output represents alternately the co-polar returns (Z) and cross-polar returns. LDR is computed simply by differencing the values of pairs of successive pulses, and summing over many pairs (the number of which is dependent on antenna beamwidth, scanning rate and PRF), followed by normalisation.

## 4. Implementation of LDR at Chilbolton:

In the case of the Chilbolton radar, the implementation of LDR is modified, since the system is also required to measure $Z_{DR}$. The arrangement is shown in Figure 2. A hybrid junction between circular and rectangular waveguides serves as a polariser. The circular waveguide port is connected to a scalar feed having five choke rings. The illumination of the dish is thus well matched in both horizontal and vertical planes, which is essential for accurate $Z_{DR}$ measurements. Furthermore, for the Chilbolton 25 m antenna, the XPD limit is sufficiently low so as to enable LDR measurements down to -34 dB. A mechanical waveguide switch based on a rotary vane is used to generate alternate horizontally and vertically polarised transmit pulses. The circulators act as transmit-receive duplexers, while the TR-cells and varactor limiters provide receiver protection. Signals from the horizontally and vertically polarised receive channels are routed to a PIN diode transfer switch, which is commutated in sympathy with the transmitted polarisation state. While the transmitted polarisation is changed from pulse to pulse (HVHVH...), one output of the PIN switch represents returns which are co-polar with the transmitted polarisation, while the other output represents the cross-polar returns. These signals ($Z_{HH}$, $Z_{VV}$, $Z_{HV}$ and $Z_{VH}$) are down-converted to I.F., log detected, digitized and processed in real-time on a DSP card to yield $Z_H$, $Z_{DR}$ and LDR. The dual-channel receiver and I.F. processor are shown in Figures 3 and 4.

*Cost-75 International Seminar on Advanced Weather Radar Systems*
*Brussels, 20-23 September 1994*
*To be published in 1995*

It might be imagined that the PIN switch preceding the dual receivers could be dispensed with, and the switching performed at I.F., rather than R.F. This seems attractive, since the switch would be considerably cheaper at low frequencies. However, one has to consider the gain stability required in the receivers for $Z_{DR}$ measurements. If I.F. switching were used, any differential gain variations between the two receiver chains would contribute directly to an error in the measured $Z_{DR}$. Drop size distributions inferred from $Z_{DR}$ are sensitive to errors of the order of 0.1 dB, so we see that the receiver gains would have to track each other with respect to, say, temperature drift, to this degree of accuracy. This is a formidable problem. However, if we use R.F. switching at the receiver inputs, we can use one channel to process $Z_{HH}$ and $Z_{VV}$. In this case, the receiver gain needs only to maintain stability over the interpulse period, and this is easily attained. Differential gain errors between the two receiver channels will only effect LDR: however, since the precision required for LDR measurements is around 1 dB, this is much less of a problem. In any event, the absolute and relative gains of both the receiver channels are periodically checked by injecting a signal from a calibration oscillator. This ensures that the measured $Z_H$, $Z_{DR}$ and LDR are largely independent of small changes in receiver characteristics. Observations of randomly-polarised solar radio noise provide a further cross-check on $Z_{DR}$ and LDR measurements.

## 5. Applications of Doppler:

Clearly, Doppler radar data have several direct applications such as identification of ground clutter contamination and measurement of precipitation fall velocity, plus characterisation of wind fields. However, a further benefit of Doppler operation, in the case of a dual-polarisation radar, is the ability to measure the differential phase shift, $\emptyset_{DP}$[3]. This parameter provides another means of distinguishing ice from water, identifying the melting layer, and making path-integrated measurements of rain-rate.

## 6. Methods of implementation of Doppler:

Traditionally, various approaches have been used to achieve Doppler operation. These range from magnetron systems using a re-lockable COHO, through injection locking to a fully-coherent klystron based system. Each has its own particular price-performance trade-off. We present an alternative method, which required no modifications to our existing magnetron-based transmitter, yet gives good quality Doppler and phase data. The residual phase-noise due to the magnetron is insignificant relative to the Doppler width of typical meteorological targets, so a klystron transmitter would only provide improved clutter cancellation. The technique should be generally applicable to other users of magnetron transmitters, and at low cost.

## 7. Implementation of Doppler at Chilbolton:

In order to make successful Doppler measurements with an incoherent transmitter, we need to sample the phase of the transmitted signal at a well-defined time during each emitted pulse. If these phase angles are subtracted from the phases of the radar returns in each range gate, for each transmitted pulse, then we obtain the phase contribution due to the radar targets alone. In the Chilbolton system [4], a waveguide cross-coupler is used to obtain a sample of the transmitter output. This is down-converted to I.F. by the same high-stability crystal-controlled phase-locked oscillator used to down-convert the target echoes. At the I.F.'s, both the co-polar and cross-polar receiver signals, plus the transmitter sample are I/Q detected using a programmable synthesiser as the COHO reference. The I and Q signals due to the receivers are continuously digitized, while those due to the transmitter are sampled and held at the optimum time, then digitized. 8 bit ADC's are used, sampling at 2 MHz, with FIFO data buffers. The three sets of digitized I and Q data are processed by an MM96-based DSP card in order to obtain the required phase angles. Pulse-pair processing on the DSP yields the mean Doppler velocity and the differential phase. The DSP card is resident in a PC, which controls the data

acquisition timing and runs a 'C' program implementing real-time colour display. The data acquisition system, which is also used for the processing and display of the $Z_H$, $Z_{DR}$ and LDR data, is shown in Figure 5.

## 8. Cost of upgrading existing radars:

The approximate costs of adding the extra hardware required to achieve LDR and Doppler operation for the case of a magnetron-based single linear-polarised reflectivity radar are shown in Table 2. We assume S or C band operation, and a common I.F., such as 30 MHz. Most components are available off-the-shelf from a variety of manufacturers. Only the costs of the microwave and I.F. hardware are considered, since data acquisition and display systems tend to be user-specific. However, as a guide, the hardware cost of the ADC's, DSP's, PC's and ancillary control, timing and interface electronics did not exceed 25K ECU in our case.

## 9. Example data:

Figure 6 shows an example of LDR data taken with the Chilbolton radar. Note the ground clutter contamination at short range is clearly shown, as is a clear indication of the presence of the melting layer. Figure 7 shows an example of Doppler data. Again, note the ground clutter and the variation of radial velocity as a function of antenna azimuth in the rain. The $\emptyset_{DP}$ data show a gradual increase in phase through the rain, a noisy region in the melting layer (due to the low correlation between the $Z_{HH}$ and $Z_{VV}$returns), and a rapid increase in phase in the ice region.

## 10. Conclusion:

This paper has reviewed the benefits of LDR and Doppler measurements, their general implementation and specific details of the schemes used on the Chilbolton radar. Costs were presented for upgrading existing radars, and some example data briefly described.

## 11. Acknowledgements:

The Doppler development at Chilbolton was supported by NERC grants GR3/7618 and 8523. The U.K. Radiocommunications Agency contributed to the running costs of the radar. We acknowledge the contributions of our colleagues at RAL and JCMM to the work reported here.

## 12. References:

[1] 'The Chilbolton Advanced Meteorological Radar' by Goddard, J.W.F., Eastment, J.D. and Thurai, M. IEE Electronics and Communication Engineering Journal, April 1994.

[2] 'Polarisation radar estimates of rainfall: Correction of errors due to the bright band and to anomalous propagation' by Caylor, I.J. and Illingworth, A.J. COST 73 Seminar, Ljubljana, Yugoslavia, 1991.

[3] 'Differential phase measurements of radar returns from precipitation' by Li, H., Blackman, T.M., Eastment, J.D. and Illingworth, A.J. Proceedings of URSI Symposium on Wave propagation and remote sensing, June 1992, p 4.4.1-4.4.6.

[4] 'A simple method of Dopplerizing a pulsed magnetron radar' by Li, H., Illingworth, A.J. and Eastment, J.D. Microwave Journal, April 1994, p 226-236.

TABLE 1

SPECIFICATION OF THE CHILBOLTON RADAR

Specification

| | |
|---|---|
| Frequency | 3.0765 GHz |
| Power | 0.5 MW |
| Pulse width | 0.5 usec (75 m) |
| Repetition rate | 610 Hz |
| Receiver Noise Figure | 1.3 dB |
| Total system noise | 4 dB (includes switch and connectors) |
| Receiver bandwidth | 4 MHz |
| Antenna size | 25 m |
| Antenna gain at 3 GHz | 53.5 dB (including feed losses) |
| Antenna mount type | Azimuth/elevation mount |
| Maximum scanning rate | 1°/second |
| Beamwidth at 3 GHz | 0.25° |

Polarisation:

| | |
|---|---|
| Transmit | Pulse to pulse switching V and H |
| Receive | Simultaneous co and cross polar |
| Cross-Polar Antenna isolation | -34 dB |

Recording and dynamic range:

| | | | |
|---|---|---|---|
| Digitisation rate | | | 2 MHz |
| Maximum range | | | 160 km |
| Reflectivity via logarithmic amplifier: | | | |
| - co-polar | dynamic range | 96 dB | (9 bits, 0.25 dB/bit) |
| - cross-polar | dynamic range | 80 dB | (8 bits, 0.5 dB/bit) |
| Doppler via limiting amplifier: | | | |
| | dynamic range | 80 dB | (8 bits for I and Q) |

Under normal scanning conditions (1°/second and 300 m gates) the following accuracies are obtained:

| | |
|---|---|
| Absolute reflectivity | 0.75 dB |
| Sensitivity at 10 km | -24 dBZ (S/N unity, dwell 0.25 sec) |
| Differential reflectivity | 0.125 dB |
| Cross polar return | 0.75 dB |
| Maximum Unambiguous Doppler | ± 15 m/s |
| Phase | 0.5° |
| Differential phase (H-V) | ±0.5° |
| Mean Doppler velocity | ±0.05 m/s |

TABLE 2

**Cost of upgrading existing radars**

for LDR:

| Extra component | Cost/K ECU |
|---|---|
| Scalar feed | 3.5 |
| OMT | 1.5 |
| Receiver protection, extra channel | 0.7 |
| PIN switch | 2.0 |
| | 7.7 |

Pre-requisite: good antenna XPD. (20 dB or better)

for Doppler:

| Extra component | cost/K ECU |
|---|---|
| Waveguide cross-coupler | 1.5 |
| Downconverter for Tx sample | 3.0 |
| I/Q detectors | 2.0 |
| COHO synthesizer | 2.0 |
| I.F. amplifiers and power splitters | 2.5 |
| Sample and hold + timing circuitry | 0.7 |
| High-performance STALO | 2.5 |
| | 14.2 |

Figure 1: (a) Single Linear Polarisation Reflectivity Radar

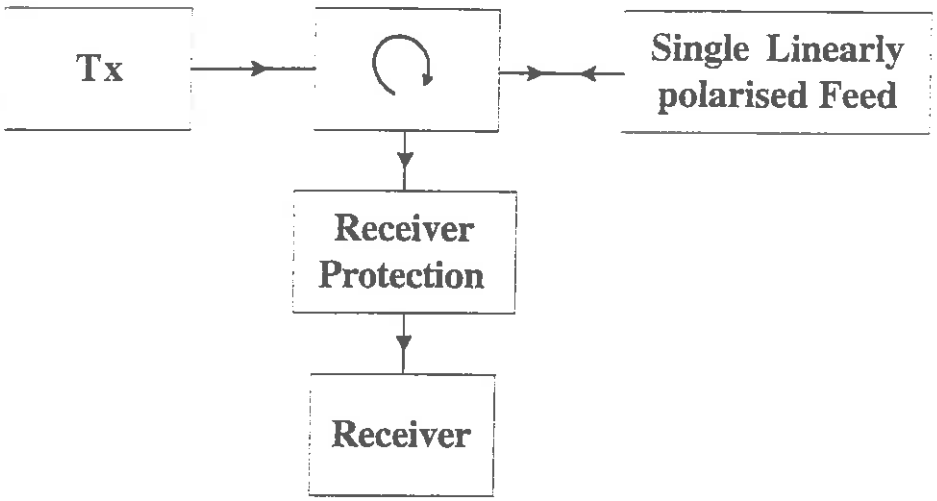


Figure 1: (b) Radar Modification for LDR Capability

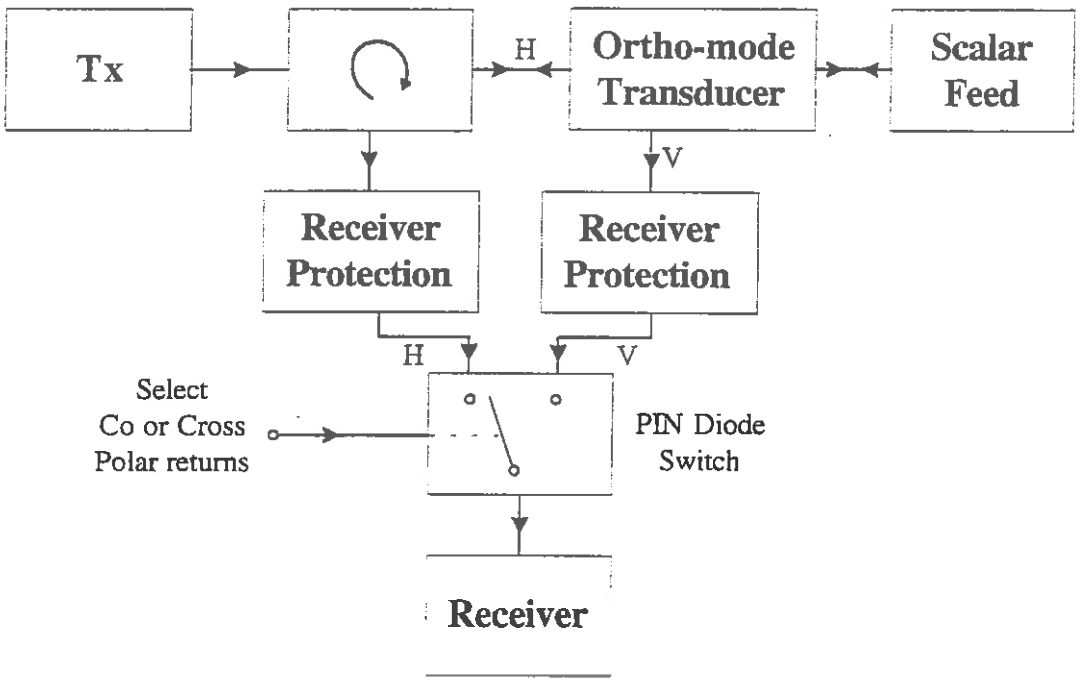

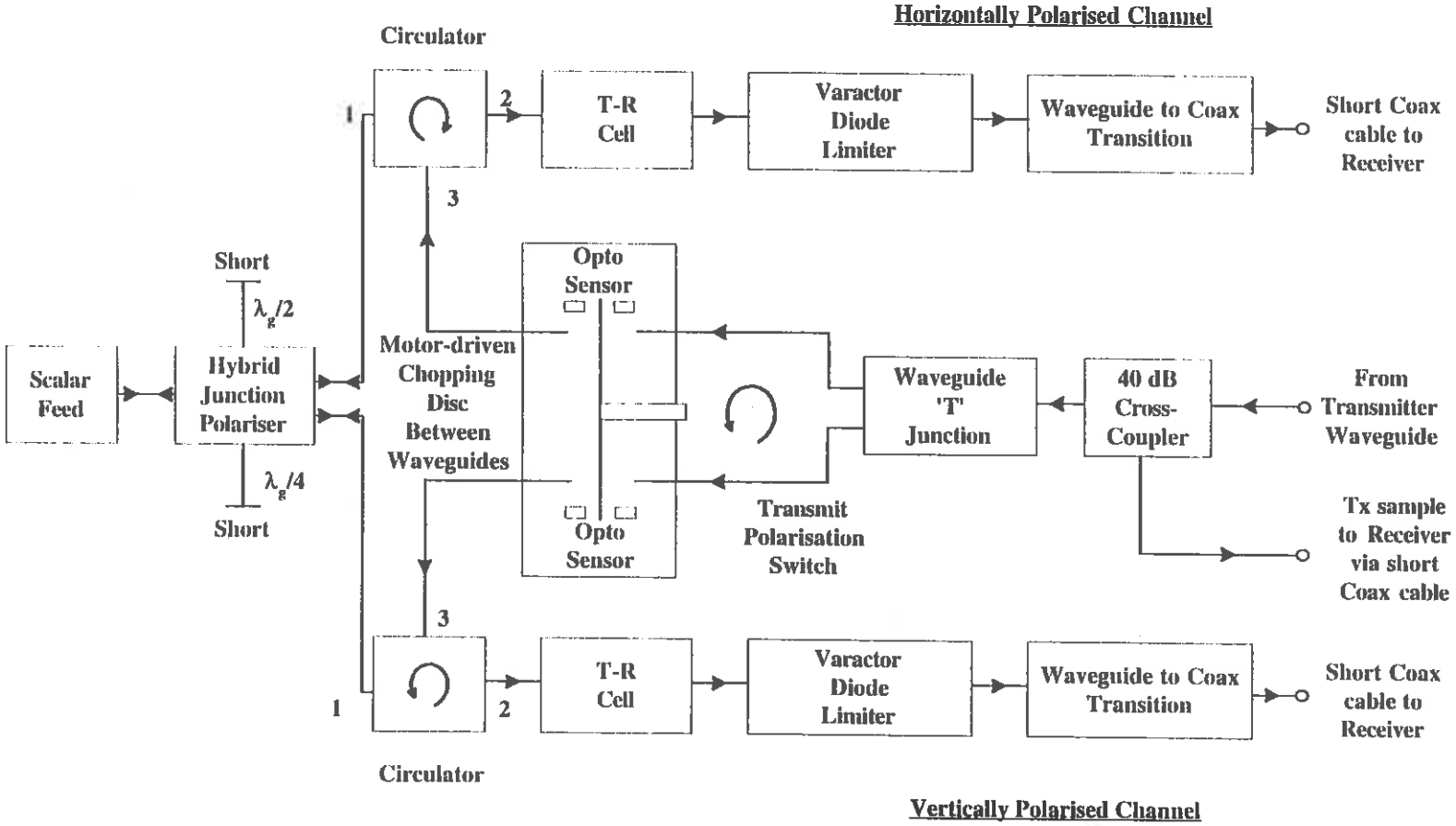


Figure 2: Polariser Assembly

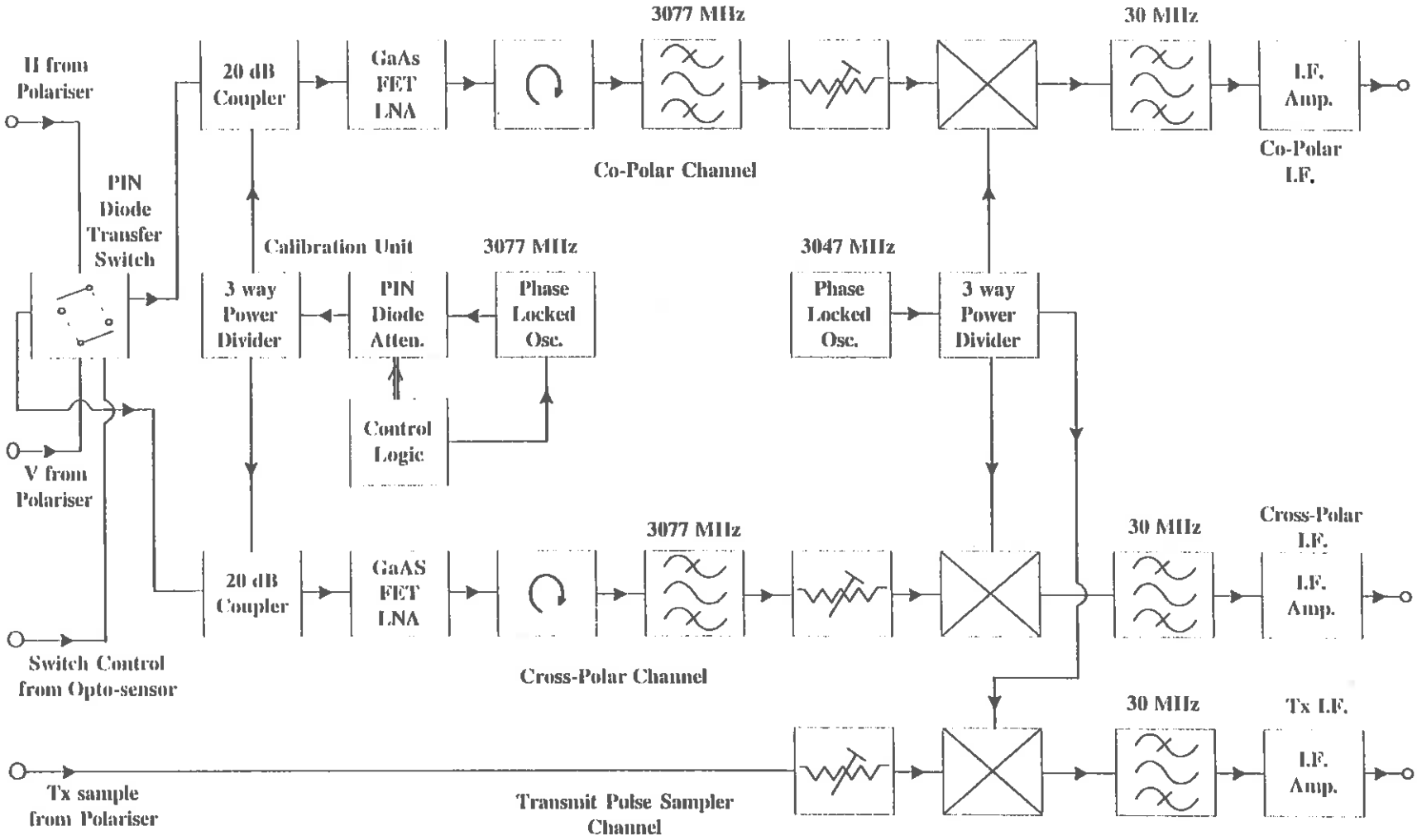


Figure 3: Dual-Channel Receiver

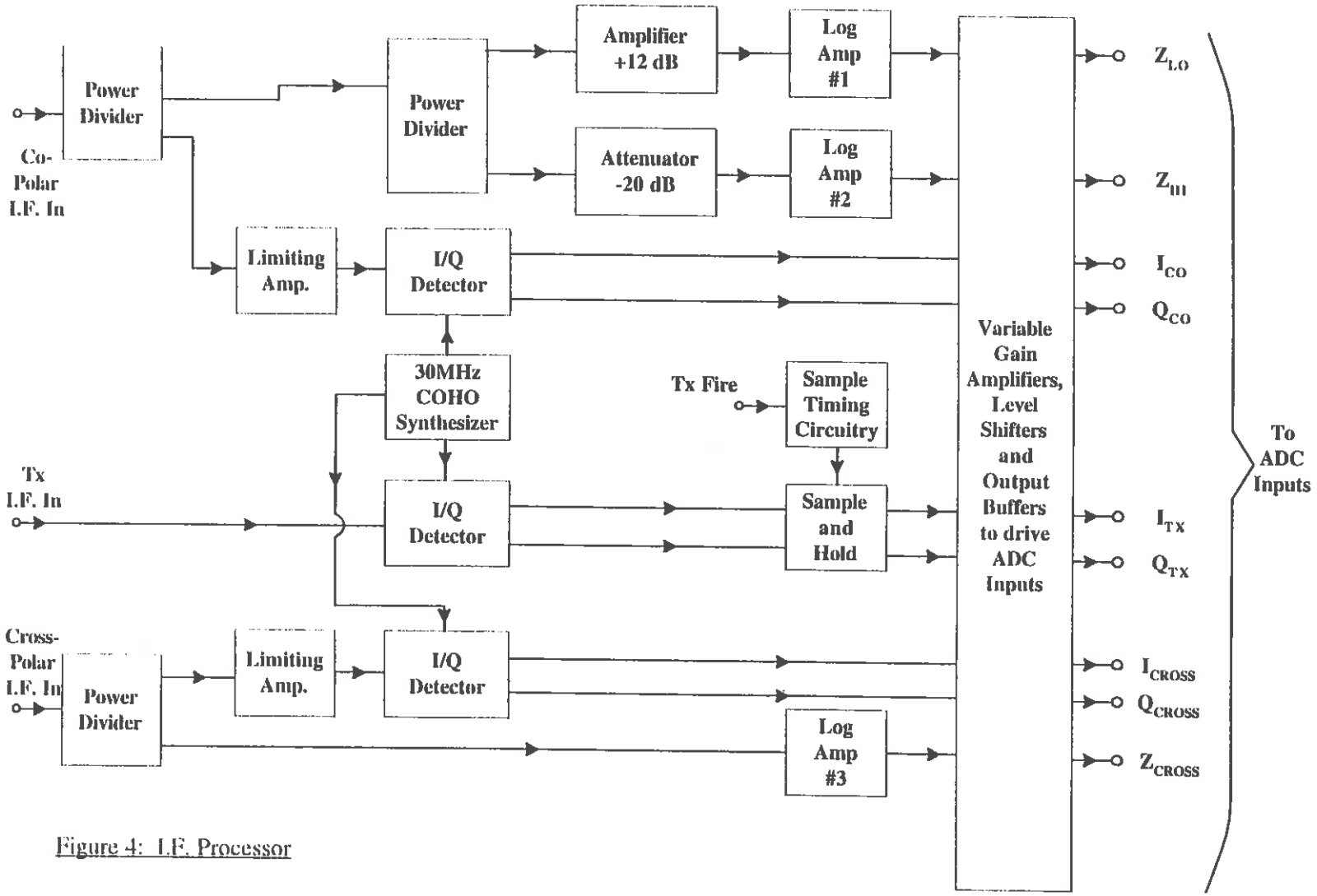


Figure 4: I.F. Processor

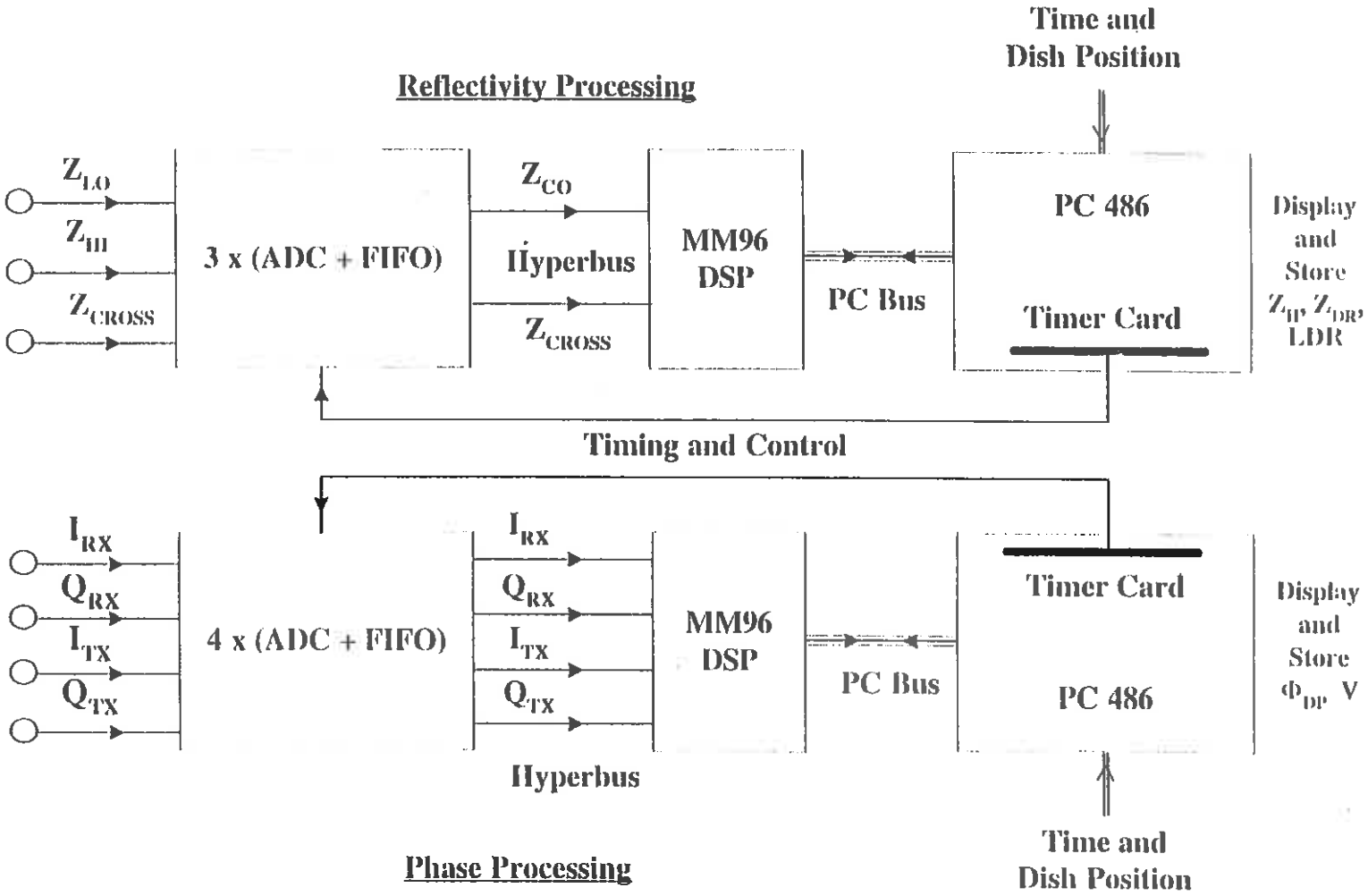


Figure 5: Data Acquisition System

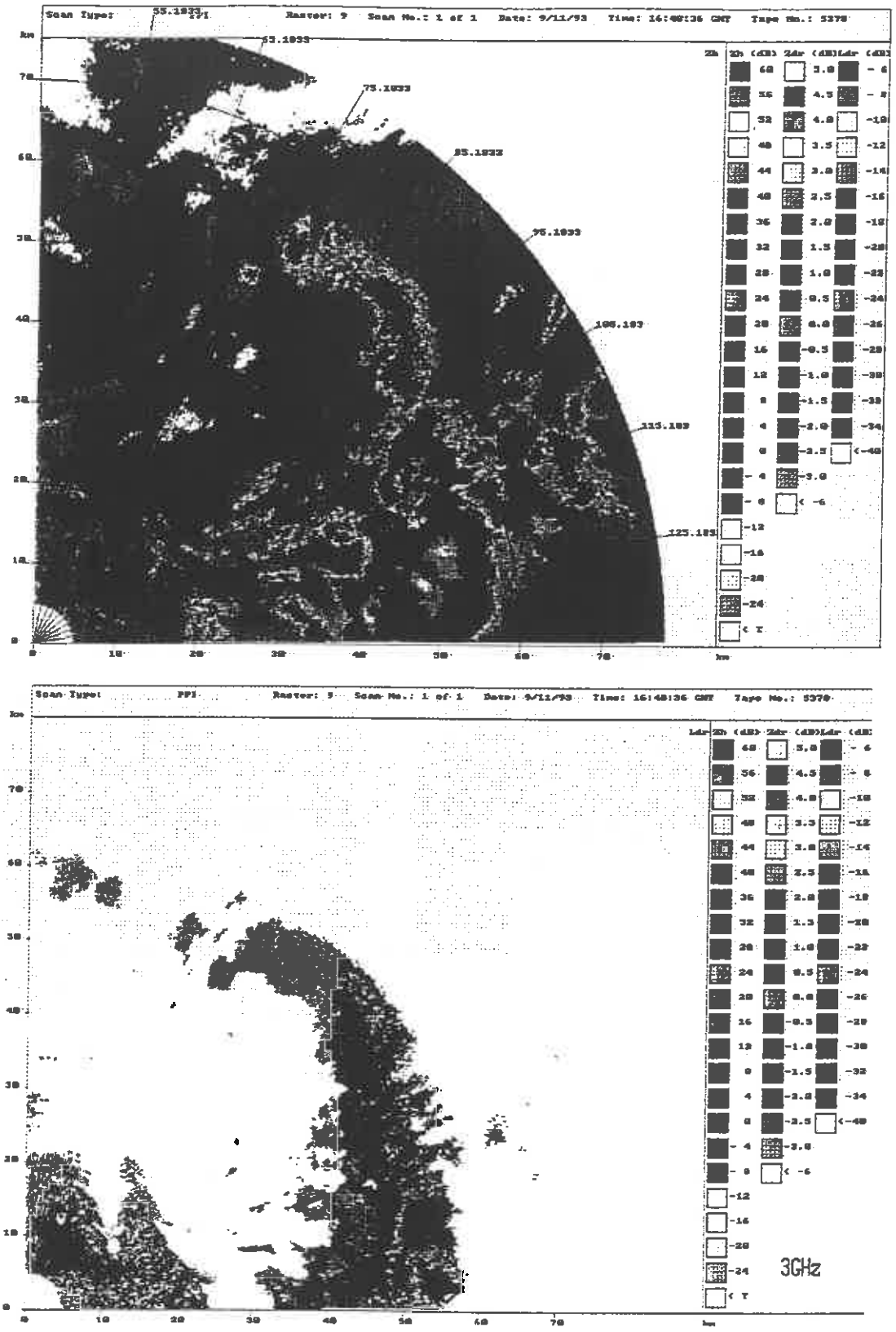


Figure 6: Reflectivity (top) and Linear Depolarisation Ratio (bottom) on 9th November 1993

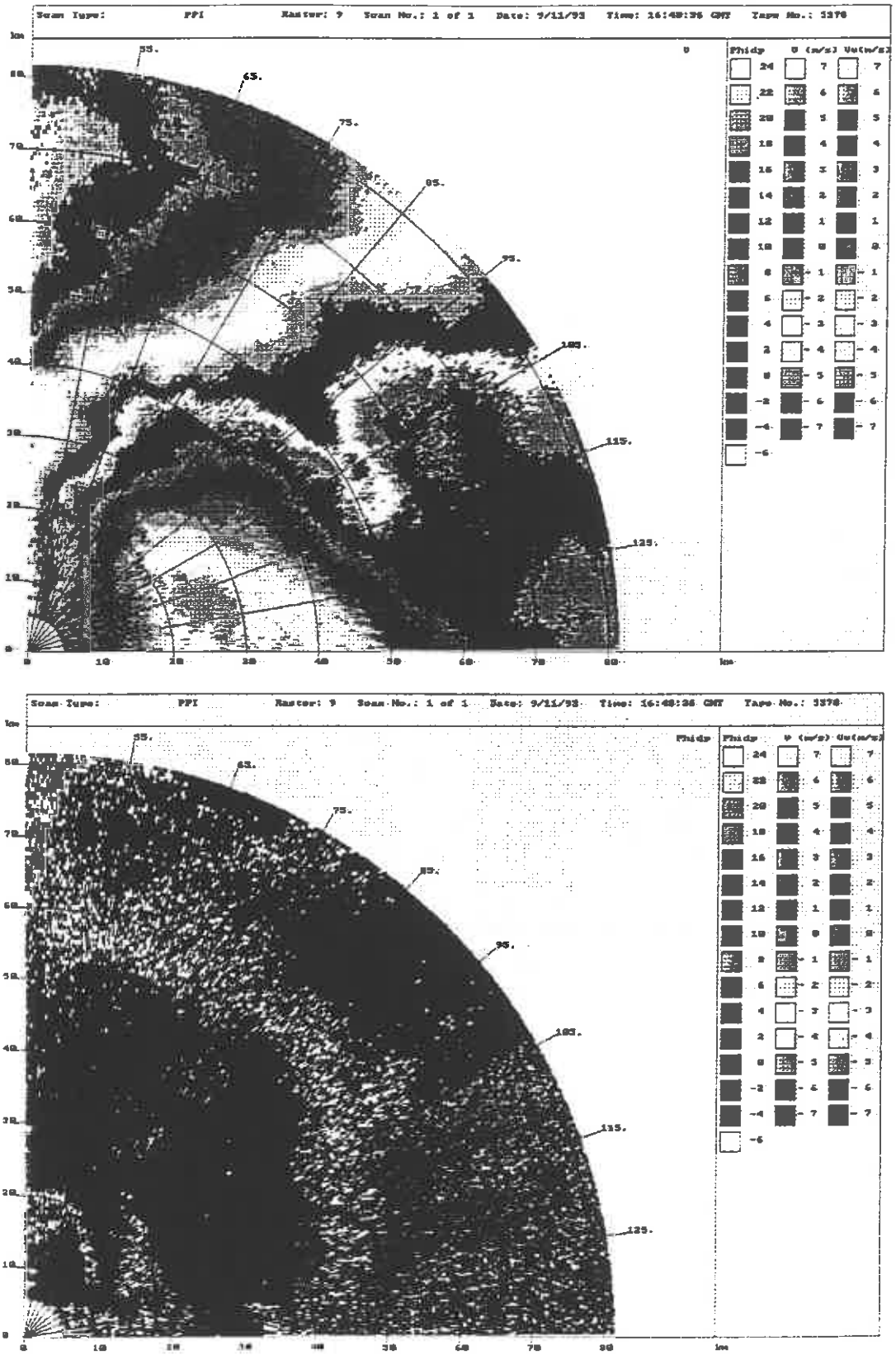

Figure 7: Doppler Velocity (top) and Differential Phase (bottom) on 9th November 1993

## CURRENT JCMM INTERNAL REPORTS

This series of JCMM Internal Reports, initiated in 1993, contains unpublished reports and also versions of articles submitted for publication. The complete set of Internal Reports is available from the National Meteorology Library on loan, if required.

1. **Research Strategy and Programme.**
   K A Browning et al
   January 1993

2. **The GEWEX Cloud System Study (GCSS).**
   GEWEX Cloud System Science Team
   January 1993

3. **Evolution of a mesoscale upper tropospheric vorticity maximum and comma cloud from a cloud-free two-dimensional potential vorticity anomaly.**
   K A Browning
   January 1993

4. **The Global Energy and Water Cycle**
   K A Browning
   July 1993

5. **Structure of a midlatitude cyclone before occlusion.**
   K A Browning and N Roberts
   July 1993

6. **Developments in Systems and Tools for Weather Forecasting.**
   K A Browning and G Szejwach
   July 1993

7. **Diagnostic study of a narrow cold frontal rainband and severe winds associated with a stratospheric intrusion.**
   K A Browning and R Reynolds
   August 1993

8. **Survey of perceived priority issues in the parametrizations of cloud-related processes in GCMs.**
   K A Browning
   September 1993

9. **The Effect of Rain on Longwave Radiation.**
   I Dharssi
   September 1993

10. **Cloud Microphysical Processes - A Description of the Parametrization used in the Large Eddy Model.**
H Swann
July 1994

11. **An Appreciation of the Meteorological Research of Ernst Kleinschmidt.**
A J Thorpe
May 1992

12. **Potential Vorticity of Flow Along the Alps.**
A J Thorpe, H Volkert and Dietrich Heimann
August 1992

13. **The Representation of Fronts.**
A J Thorpe
January 1993

14. **A Parametrization Scheme for Symmetric Instability: Tests for an Idealised Flow.**
C S Chan and A J Thorpe
February 1993

15. **The Fronts 92 Experiment: a Quicklook Atlas.**
Edited by T D Hewson
November 1993

16. **Frontal wave stability during moist deformation frontogenesis. Part 1. Linear wave dynamics**
C H Bishop and A J Thorpe
May 1993

17. **Frontal wave stability during moist deformation frontogenesis. Part 2. The suppression of non-linear wave development.**
C H Bishop and A J Thorpe
May 1993

18. **Gravity waves in sheared ducts.**
S Monserrat and A J Thorpe
October 1993

19. **Potential Vorticity and the Electrostatics Analogy: Quasi-Geostrophic Theory.**
C Bishop and A J Thorpe
November 1993

20. **Recent Advances in the Measurement of Precipitation by Radar.**
A J Illingworth
April 1993

21. **Micro-Physique et Givrage. Cloud Microphysics and Aircraft Icing.**
A J Illingworth
May 1993

22. **Differential Phase Measurements of Precipitation.**
M Blackman and A J Illingworth
May 1993

23. **Estimation of Effective Radius of Cloud Particles from the Radar Reflectivity.**
N I Fox and A J Illingworth
May 1993

24. **A Simple Method of Dopplerising a Pulsed Magnetron Radar.**
L Hua, A J Illingworth and J Eastment
November 1993

25. **Radiation and Polar Lows.**
George C Craig
February 1994

26. **Collected preprints submitted to International Symposium on the Life Cycles of Extratropical Cyclones; Bergen, Norway, 27 June - 1 July 1994**
April 1994

27. **Convective Frontogenesis**
Douglas J Parker and Alan J Thorpe
April 1994

28. **Improved Measurement Of The Ice Water Content In Cirrus Using A Total Water Evaporator**
Philip R A Brown and Peter N Francis
April 1994

29. **Mesoscale Effects of a Dry Intrusion within a Vigorous Cyclone**
K A Browning and B W Golding
April 1994

30. **GEWEX Cloud System Study, Science Plan**
May 1994

31. **Parametrization of Momentum Transport by Convectively Generated Gravity Waves**
R Kershaw
May 1994

32. **Mesoscale Modelling Newsletter, No. 5**
May 1994

33. **Observations of the mesoscale sub-structure in the cold air of a developing frontal cyclone**
K A Browning, S A Clough, C S A Davitt, N M Roberts and T D Hewson
May 1994

34. **Longwave Radiative Forcing of a Simulated Tropical Squall Line**
Imtiaz Dharssi
July 1994

35. **On the nature of the convective circulations at a kata-cold front**
K A Browning
September 1994

36. **Collected preprints of papers submitted to the COST-75 International Seminar on Advanced Weather Radar Systems, Brussels, 20-23 September 1994**
November 1994

**Met Office** Joint Centre for Mesoscale Meteorology Department of Meteorology
University of Reading PO Box 243 Reading RG6 6BB United Kingdom
Tel: +44 (0)118 931 8425 Fax: +44 (0)118 931 8791
www.metoffice.com